SAPIENZA
UNIVERSITÀ DI ROMA

Archaeometallurgical characterisation of ancient Roman bronze coins

Facoltà di Scienze Matematiche, Fisiche e Naturali

Corso di laurea in Scienze e Tecnologie per la Conservazione dei Beni Culturali

Erasmus Mundus Master in Archaeological Materials Science (ARCHMAT)

Candidato

Nome e Cognome Elizaveta Demidova

n° matricola 1723217

Relatore

Giovanni Ettore Gigante

Correlatore

Emma Angelini

A/A 2015/2016

Contents

Introduction

The three of several ancient bronze coins were selected for this master thesis research. The coins were considered to belong to the Roman mint of the Egyptian origin in the province of Alexandria. They were excavated in the archaeological site Bubastis ancient city. Archaeometallurgical characterisation of those coins implies to a performance of detailed investigation of the chemical composition and microstructure of the alloy and the analysis of corrosion products of the coins. The archaeometry analysis was performed by means of a multi-analytical approach: X-ray diffraction (XRD), X-ray fluorescence (XRF), optical microscopy (OM), scanning electron microscopy (SEM) and energy dispersive spectrometry (EDS) will be used to determine the elemental composition and microstructure of the bulk metal and understanding the corrosion mechanism.

The origin of the three ancient bronze coins that were chosen for performing the present master thesis research is not known for sure. They are a part of a several coins collection that were purchased at a market in Egypt in Cairo with a purpose of their material study in sense of advantages of conservation science and archaeometry. It is known that nowadays it is not easy to acquire samples of historical value to perform a scientific research, taking in consideration the situation with some museums laws, that sometimes or usually do not support an idea of cooperation between cultural heritage protection and conservation science. On the other hand, a research on material study in most usual cases requires destructive methods of analysis by application of some analytical techniques that consider sample preparation (like cross-sections). 'It is often difficult to persuade museum curators to permit any sampling technique that involves the physical removal of metal from a coin, although all relevant techniques require the removal of at least some material in order to obtain or expose the 'heart metal' of the coin…' [1] [1] Obviously, the chance of destruction of cultural heritage object is not in any case acceptable, which is one of the reasons of absence of contact between museums and archaeometry and conservation science. In this case, it was necessary to find other ways of obtaining the samples, and the simple idea of their purchase was quite essential.

The provenance of the studied coins before the purchase suggests that they were excavated in Tell Basta archaeological site, which is ancient Egyptian city Bubastis and located in a Delta region of Nile, not far from modern Zagazig city (around 80 kilometers). The name of the site was originated from a cult of Egyptian cat-goddess Bastet. The archaeological site is famous by findings of numerous stone monuments and different statues. However, there was a previous study of metal objects found in the same site, carried out by researchers Ghonein M. and Megahed M. and presented at an International conference on Mediterranean Cultural Heritage in 2009 [2] [2]. The study was based on chemical composition and corrosion analysis of 25 silver coins that were excavated

[1] [1] K. Butcher and M. Ponting, "THE ROMAN DENARIUS UNDER THE JULIO-CLAUDIAN EMPERORS : MINTS , METALLURGY AND TECHNOLOGY," vol. 24, no. 2, pp. 163–197, 2005.

[2] [2] M. Ghonein and M. M. Megahed, "Treatment and conservation of a group of roman coins discovered in Tell Basta, Egypt," in *4th International Congress on Science and Technology for the Safeguard of Cultural Heritage in the Mediterranean Basin*, 2009.

in Bubastis in 1998. This research has a special importance due to the corrosion study, since the environment and burial conditions could be very similar with those of the bronze coins analysed in this thesis work.

The first aim of this research is characterisation of bulk metal alloy of the coins applying the combination of several methods. One method is a determination of chemical elemental composition with analysis of coins using X-ray fluorescence and SEM-EDS techniques, providing the qualitative and quantitative results. Another method of alloy characterisation is the metallographic examination of bulk alloy by chemical etching experiments and an application of a metallographic microscopy observation for an alloy phases' identification.

The second aim of the research is characterisation of surface patina products of the coins by the following methods: strata-graphical observation of patina was carried out by using an optical and metallographic microscopy imaging, and also with SEM-EDS imaging; the composition of corrosion products is determined by analysis that were made with XRD, μXRD and SEM-EDS techniques, comparing the results received from all the analytical techniques application, in order to obtain a reliable information and knowledge on the analysed object.

The study of patina of ancient Roman bronze coins from Alexandria can bring more light on understanding of the corrosion mechanism itself as an interesting and complex chemical phenomenon. The numerous combination of environmental factors reflect on processes of mineralisation and corrosion layers formation, that also depends on multiplicity of copper, tin and lead compounds occurred on the metal surface in result of different interactions between metal and environment. Study and identification of corrosion formation mechanism may help the conservators to understand more deeply the deterioration processes occurred in metals and to find solutions of prevention further destruction changes in an artefact.

The general results of the research analysis bring the importance to a specific field of numismatic studies, making possible to answer some question concerning historical issues of the ancient coinage.

The quantification of the main alloy elements and their compositional data can give a clue to understanding of processes of devaluation in ancient Roman times (in particular, the times during production of the certain analysed coins, from 2nd to 3rd centuries AD), concerning the provincial coinage of Alexandria as a part of Roman Empire. Devaluation is an essential subject of economic life of any developed society, especially ancient society, when every change in a precious metal content, as gold and silver, had a straight influence on a general economic stability in an ancient society. However, the compositional ratios of non-precious metals (copper, tin and lead), and their affect on a weight variations, are considered to be another factor of impact, sensitive to economic raises and declines. That is the reason why the study of coin alloy composition is able to provide useful information about history of economy problems in ancient Roman society.

The coinage of Roman Alexandria was based on the Ptolemaic system, established since the rule of Octavian in 30 B.C. with the possession of Egypt, controlled and correlated with the coinage in Rome. It was a closed currency system, isolated from other parts of Mediterranean world and Roman Empire, when local money was not permitted to leave abroad, as well as foreign currency was prohibited to enter[3]. Subsequently, Alexandrian coinage system underwent different reformations during the rule of such emperors as Augustus, Tiberius, Nero, Domitian, Trajan,

[3] The coinage of Roman Alexandria. - http://www.coinsofromanegypt.org/html/library/NFA/NFA_91_sale.htm

Antoninus Pius and other Antonine emperors. Since the period of Diocletian in 296 AD the coinage system was changed to a new unification comprised the whole empire, and all the old Alexandrian coins disappeared. Tetradrachma was a bronze coin with a light silver content, and drachma typically was minted of a bronze alloy. A special kind of a large bronze drachma denomination created and raised during the Antonine's dynasty period (138-193 AD) and was equivalent to a Roman sestertius (the type which is analogous to the *Coin_1*).

The nature of Alexandrian coins was of a special type, that however had features common for Roman provincial coinage, like that the obverse usually depicted the portrait of an emperor or of someone from his family. But the reverse varied in many depiction types known only in Egypt. 'It is the characteristic Alexandrian types, with their exotic flavor, that lend real charm to the Romano-Egyptian coinage. Counted among such types are Greco-Egyptian deities and cult symbols, centering on the myth cycle of Sarapis; depictions of the Nile, his consort Euthenia, and their cult symbols or related paraphernalia (such as the Nilometer which measured the annual innundation); the personification of Alexandria; representations of local architecture, especially the great lighthouse of Alexandria; a few ancient Egyptian deities; and native animals. These multifarious types were not employed to appeal alternately to the Greek or Egyptian elements of the population, as Milne so quaintly theorized. Rather they are an expression of local piety and patriotism, much like their counterparts on Greek imperial coinage elsewhere' [4].

The thesis work is organized in five parts. The chapter Macroscopic observation includes a numismatic description and the coins' possible provenance identification, and the historical outline. In Experimental part of this work the sample preparation is represented in details, and the techniques used for carrying out all the analysis are discussed. The part Results and discussion reports the combined results obtained with all the experimental work and their most probable meaning is discussed.

[4] The coinage of Roman Alexandria. - http://www.coinsofromanegypt.org/html/library/NFA/NFA_91_sale.htm

Macroscopic observations

The macroscopic observations of the 3 coins (samples of Coin_1, Coin_3 and Coin_4) were made in order to examine the visible characteristics and provide the numismatic description and evaluation.

The weight and dimensions of the Coin_1, Coin_3 and Coin_4 are measured and presented in a Table 1.

Table 1. The measured dimensions and weight of the coins

Coin #	Maximum diameter (mm)	Minimum diameter (mm)	Weight (g)
Coin_1	29	26	18.9380
Coin_3	18	17	10.5498
Coin_4	20	18	10.6539

Coin_1

Figure 1. Coin_1, obverse.

The *Coin_1* is the largest bronze coin from all the four, and it is less corroded than the others are, and it is less worn, that makes possible the identification of depicted figures from both sides, obverse and reverse. However, the legend of the coin is mostly disappeared.

Figure 2. Coin_1, reverse

According to the consultation and reference of Gilles Bransbourg, a specialist in the monetary and fiscal history of Greco-Roman Mediterranean World and adjunct curator of Roman Coins at the American Numismatic Society[5], the *Coin_1* most probably belongs to a type of a bronze drachm minted under rule of Antoninus Pius Emperor (86-161 AD) in Alexandria, Egyptian province of Roman Empire. Although the size and weight are slightly low in comparison with other coins of the same type, however, some samples match those dimensions, like the present example does.

Obverse depicts His laureate profile turned on the right. Reverse: Isis Pharia is standing right and holding a billowing sail.

There are some important facts to know about Isis Pharia, the figure of which is quite common to see depicted on Roman coins of the Egyptian origin.

[5] http://numismatics.org/

Isis Pharia was the main goddess of Alexandria, which, according to Pliny[6], was related to and named for the Great lighthouse of Alexandria, one of the seven wonders of Ancient World, that was located on Pharos island, linked by a bridge to a Roman colony in Egypt, Alexandria. 'Isis of the sea' was a guardian of navigation and a protector of the Pharos lighthouse, she was usually depicted on Roman Egyptian coins standing in front of the lighthouse, with her mantle blown behind Her shoulder and with a billowing sail in the right hand (exactly as Isis Pharia of the *Coin_1* reverse). Another variant of Her depicted on some other coins is when she holds or carries a sistrum in Her right hand, which is a kind of an ancient Egyptian metallic percussion musical instrument.

The short historical outline of Antoninus Pius biography is provided in order to link the object of this research (Coin_1) with the time of it's actual existence.

Antoninus Pius, 19 September, 86 AD – 7 March, 161 AD (lat. *Titus Aurelius Fulvus Boionius Arrius Antoninus Pius*) was a Roman Emperor, ruled from 138 till 161 AD. He was the fourth from Five Good Emperors. Originally he was from a senatorial family of Gallia-Narbonensis. In 120 AD he was a consul and later proconsul of Asia. In 135 AD he was adopted by Hadrian Emperor and became his successor. After Hadrian's death Antoninus convinced the Senate to deify him and that was the reason he has been called Pius what means 'devotional' or 'pious'.

During the ruling time of Antoninus Pius the Roman Empire maintained its possessions and strengthened the borders. By his order the defensive earthworks were done in Scotland, and also the borders with Germany and Raetia were strengthened and moved forward. However, rebellions started in provinces of Britain, in Mauritania, Egypt, Judea against the roman rule signified the soon end of stability. 'Although some sources suggest that Antoninus went in person to Egypt and Syria to put down a revolt of peoples along the Red Sea, Julius Capitolinus says that Antoninus made his home in Rome where he could receive messages from all parts of the empire equally quickly'[7].

Several images of Antoninus Pius coins, found in Roman numismatic catalogues and considered to belong to the same emperor's rule (such as Keith Emmett collection of Roman Egypt, 'Roman Imperial Coins of Antoninus Pius' virtual catalogue, 'The coinage of Roman Alexandria' virtual catalogue, and others), are represented below for the visual comparison with Coin_1, and in order to prove the evidence of the coin's origin identification correctness of Coin_1 relation with the times of Antoninus Pius rule (2nd century AD).

Figure 3 represents the Antoninus Pius AE drachm of Alexandria, which is totally identical to the Coin_1 in the sense of obverse and reverse appearance. 'Obverse: laurate, draped and cuirassed bust right, seen from right. Reverse: Isis Pharia standing right, holding billowing sail, 35mm, 24.86 grams'. However, the difference in weight is significant.

[6] Dictionary of Roman Coins. - http://www.forumancientcoins.com/Dictionary_Of_Roman_Coins/dictionaryByPage.asp?page=622

[7] Weigel, Richard D. "Antoninus Pius (A.D. 138–161) De Imperatoribus Romanis" http://www.roman-emperors.org/tonypis.htm

Figure 3. **Antoninus Pius AE drachm of Alexandria.** [8]

Figure 4. AE Drachm of Antoninus Pius, 148-149 AD.

The Figure 4 represents the coin of the virtual collection of 'Roman Imperial Coins of Antoninus Pius' with the following numismatic charecteristics: 'Egypt, Alexandria. Antoninus Pius. Year 12 (=148/9 AD). AE Drachm. AVT K T AIL ADP ANT...., laureate, draped and cuirassed bust right / Isis Pharia holding billowing sail and sistrum, walking to right toward the Pharos lighthouse'[9]

[8] Roman provincial coins/Egypt. VCoins collection. https://www.vcoins.com/en/stores/ephesus_numismatics/56/product/antoninus_pius__drachm_of_alexandria_egypt__isis_pharia_holding_sail/599953/Default.aspx

[9] Roman Imperial Coins of Antoninus Pius. http://www.wildwinds.com/coins/ric/antoninus_pius/i.html

Figure 5. AE Drachm of Alexandria, 146-147 AD.

Figure 5 shows another example of Antoninus Pius Drachm of Alexandria, the image of which was received from the same virtual collection[10], accompanied with detailed numismatic description: 'Antoninus Pius. Year 10 (=146/7 AD). AE Drachm of Alexandria. AVT K T AIL ADP ANTONINOC, laureate and draped bust right / LDЄ-KATOV, Isis Pharia standing right, holding billowing sail'.

[10] The same as above. http://www.wildwinds.com/coins/ric/antoninus_pius/i.html

Coin_3 and **Coin_4**

Figure 6. Coin_3, obverse

Figure 7. Coin_3 reverse

Figure 8. Coin_4, obverse

Figure 9. Coin_4, reverse

Coin_ 3 and Coin_4 are considered to be of the same or similar origin. This conclusion can be made by comparison of dimensions. Both coins have the same weight (around 10 g) and diameter between 18 and 20 mm. The nature of corrosion formed on the both coins is identical, according to the results of XRD and SEM-EDS analysis.

Both of the coins were very worn and in an extremely corroded state, as it it possible to see on the pictures of coins (Figures 6-9), so it was not even possible to define any image of the minting relief, no legends and symbols were readable, except of some letters on the obverse of Coin_3, that are barely visible, but still it is possible to make a guess on the origin identification,

According to the consultation and reference advise of Gilles Bransbourg, a specialist in the monetary and fiscal history of Greco-Roman Mediterranean World and adjunct curator of Roman Coins at the American Numismatic Society[11], the dimensions of Coin_3 and Coin_4 (18-20 mm of diameter and weight of 10,5-10,6 gramms) can possibly and roughly apply to a Billon Tetradrachm coin with a dating time of 235-270 AD. A letter 'M' is clearly visible on a legend field of the Coin_3 obverse, and that can link to a possible candidate of Maximinus I Thrax (173-238 AD, the Roman Emperor from 235 to 238 AD). AVTO MAXIMINO CEV CEB would be the full inscription of the legend, which cannot be subjected to a more safe interpretation since the coin was very worn and corroded. The other candidate names of Roman rulers that include the letter 'M' and could imply to the dating of Coin_3 and Coin_4 and their origin are Emperors Numerian (282-284 AD of reign), Maximian (286-305 AD of reign) or Macrianus (260-261 AD of reign). However, the provincial Egyptian coinage of Maximinus I Thrax was taken to a regard and comparison with Coin_3 and Coin_4. The following images represent coins from a virtual numismatic source of the Milne collection [12].

Figure 10. Maximinus I AE tetradrachm of Alexandria, Egypt (AD 236-7).

[11] http://numismatics.org/About/GillesBransbourg

[12] Roman Imperial Coins of Maximinus I. http://www.wildwinds.com/coins/ric/maximinus_I/i.html

On Figure 10 is a billon tetradrachm of Maximinus I from Alexandria, Egypt. Dimensions are 22mm in diameter and the weight is 12.82g. Dated Year 3 (AD 236/7). 'AVTO MAXIMINO CEVE CEB, laureate, draped, cuirassed bust right / Trophy of arms; bound captive to left and right, L-G across fields' [13].

Figure 11. Numerian, Potin Tetradrachm of Alexandria (282–283 AD).

A potin tetradrachm of Alexandria (weight 8.10 g), minted under Numerian's rule is shown on the Figure 11, dated by 282–283 AD. 'AK M A NOVMERIANOC K C, laureate, draped and cuirassed bust right / L-A, Dikaiosyne standing left, holding scales and cornucopiae; robe draped over her left arm'[14].

Figure 12. Numerian, AE tetradrachm of Alexandria (AD 284).

The weight of Coin_3 and Coin_4 which is equal to 10.54 g and 10.65 g does not coincide with the weight of both Maximinus I and Numerian coins, mentioned in the numismatic collections (12,82 g and 8.10 g), that makes the comparison more confusing, however there are other morphological characteristic concerning stylistic details of

[13] Roman Imperial Coins of Maximinus I. http://www.wildwinds.com/coins/ric/maximinus_I/i.html
[14] Roman Imperial Coins of Numerian. http://www.wildwinds.com/coins/ric/numerian/i.html

minting common between all the reviewed coins and the examined coins, that make their comparison quite reliable.

Another Egyptian bronze tetradrachm of Numerian is shown by a Figure 12. It is dated by year AD 284, and inscription of the legend written in Greek is: 'A K M AN NOVM-EPIANOC CEB', the obverse depicts His laureate draped bust right, inscription of the reverse is :'ETOVC Γ' and it has an image of Eirene (Pax) which stands left, holding olive branch and transverse sceptre[15].

Both of the 2 coins from Numerian times can be compared with the Coin_3 sample, since there is that similar characteristic – the ornamented frame between the legend and the edge of coin. This characteristic belongs to the general coinage style of the 3rd century AD, that can be observed through examples of provincial coinage of Maximianus I, Numerius and Maximinus, that are made in this work for comparison. Another common characteristic of those times coinage is the typical style of font used in minting for legend inscriptions.

The coin of Maximian (286-305 AD of reign) is shown on a Figure 13, which is another example of the characteristics described above. The legend of the obverse says 'IMP C VAL MAXIMIANVS P F AVG' and depicts His laureate head right. Reverse: 'GENIO POPVLI ROMANI S-P' with 'Genius standing left, modius on head, pouring libations from patera and holding cornucopiae to right'[16](cornu copiae - horn of plenty, is a symbol of abundance and nourishment).

Figure 13. Maximianus AE Follis. 302-303 AD.

Experimental

Sample preparation

- Cutting the fragments

[15] Roman Imperial Coins of Numerian. http://www.wildwinds.com/coins/ric/numerian/i.html
[16] Roman Imperial Coins of Maximianus. http://www.wildwinds.com/coins/ric/maximianus/i.html

Small area on each of four coins was selected to be removed in order to prepare cross-sections in a resin for the further analysis with such analytical techniques as Optical and Metallographic Microscopy. The choice of fragment to cut depended on amount of corrosion products that are located close to any edge of coin diameter, with the purpose of less damage of the object, so the main numismatic information, still remained on some of the sides on several coins, will not be destructed by mechanical impact of sample preparation.

The selected fragment of the *Coin_1* (Figure 14) was the only area with high amount of corrosion located on the edge at the lower part of side A (obverse), it was around 1 cm of size.

Figure 14. Coin_1 after cutting procedure, obverse and reverse (A, B)

Figure 15. Coin_1 sampling cut fragment

The Coin_1 fragment after cutting procedure, selected for the cross-section sampling, is shown on the Figure 15.

The cutting area of the *Coin_3* was not hard to define, since it is completely corroded, however some significant traces of legend are still presented on the side A (obverse). The small area from the lower edge of side A was chosen to be removed.

The *Coin_4* was in a worse condition than *Coin_3*, because no coinage signs can be readable or observed, and the area for cutting was chosen from the right edge of side A, since that area had a spot of higher patina concentration in comparison with other possible areas to remove.

Figure 16. Coin_4 after cutting procedure, obverse and reverse (A, B).

Figure 17. Coin_4 sampling cut fragment.

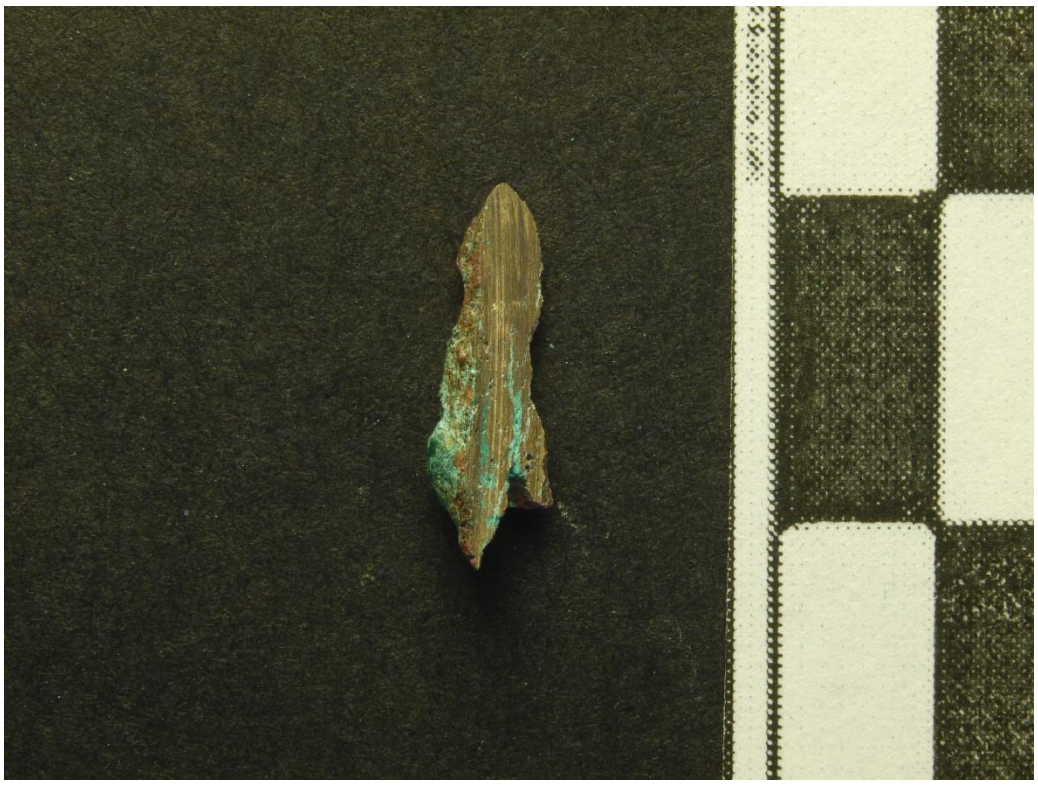

- Cutting with the saw

In order to perform an accurate and fast cross cut of coin fragments the miter saw Micromet Evolution was applied with a cutting Remet disk (125x0,5x20), set as a blade and fixed vertically under the angle of 90^0. The setup of saw constructed in a way that for the cross cut performance the sample holder is manually moved in a controlled motion with controlled pressure towards the cutting disk, while it rotates with a controlled speed, with a supply of water mixed with technical oil in order to provide efficiency of the cutting procedure, therefore all the work piece is held behind a transparent plastic fence.

The each coin was properly fixed in a sample holder in a special position towards the blade, so the blade was expected to pass through the object separating it in a line which divides the area of choice for the further cross-section preparation from the object itself.

Figure 18. Coin_3 obverse after damaging the coin during cutting procedure

During the cross cut of the *Coin_3*, the accident happened resulted in a breakage of the object and the cutting disk both, most probably because of a mistake made in fixation of the object in a sample holder, whether because of sample holder fixation on a workpiece. The *Coin_3* crashed in two large pieces and several smaller fragments, one of which was chosen for preparing a cross section for following analysis (images of obverse and reverse of damaged Coin_3 on Figures 18 and 19).

Figure 19. Coin_3 reverse after damaging the coin during cutting.

Figure 20. Coin_3 fragment of sampling

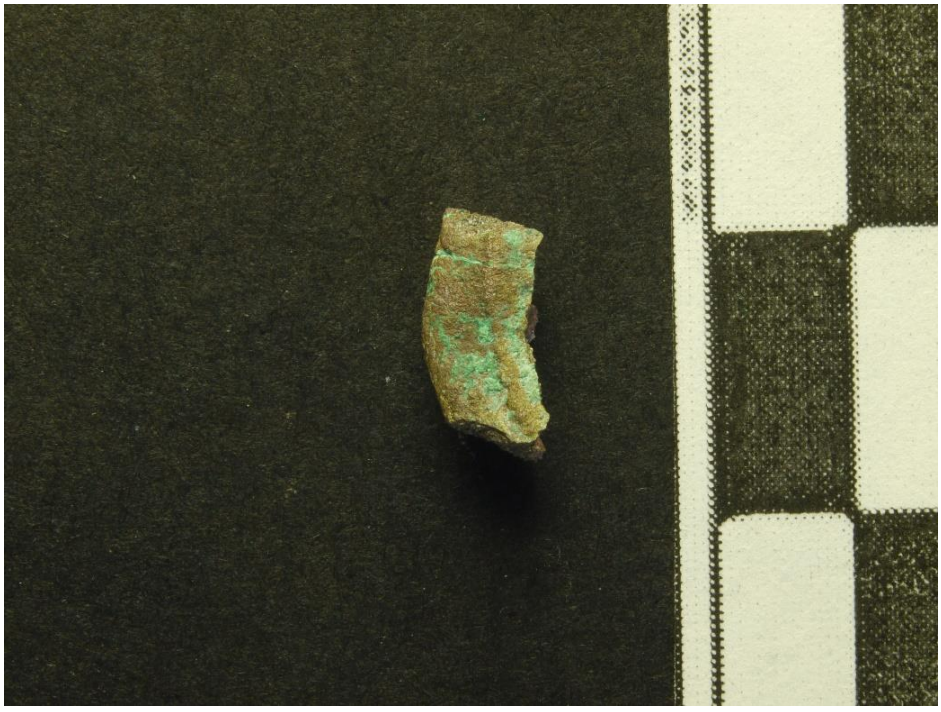

Figure 20 shows the fragment selected for the cross-section sampling occurred after damaging the coin during cutting procedure.

- Ultrasonic cleaning

After the fragments were separated from objects, they (coins and cut fragments) were subjected to a cleaning in an ultrasonic bath in order to remove any organic contamination presented on the surface of coins and oil residues remained after the use of the miter saw for cross cutting of the objects.

The principle of ultrasonic cleaning can be explained by a process of high frequency pressure waves created by ultrasound, that agitate the liquid and produce large amount of microscopic cavitation bubbles that explode with a high energy. This process result in ability of efficient cleaning of diverse objects, metallic in the present case.

The tank of ultrasonic cleaner was filled with a tap water. Each object was placed in a separate glass vessel, which was filled with a cleaning chemical solvent and after placed into the tank of ultrasonic cleaner. The use of chemical detergent solvent increase the efficiency of cleaning procedure.

Cleaning process consisted of two phases, involved a change of cleaning solvent. During the first phase the 2-propanol (isopropyl alcohol 99.5%, Sygma-Aldrich production) was used as a detergent, and for the second phase of cleaning solvent was changed to ethanol. Each cleaning was performed in duration of 15 minutes, with conditions of normal room temperature.

After all the objects have been cleaned, they were dried, wrapped in a paper and placed into a plastic bag.

- Resin sample mounting

The next step to cross sections preparation was *placing the cut coin fragments into the resin mix* in a needed position that enables their further observation in the most efficient way under the Optical and Metallurgical microscopy.

The resin used for mounting the samples is cold mounting two-component auto-polymerising resin Mecaprex KM-U, consisted of two components: liquid resin and the powder, that were mixed together rapidly in a ceramic vessel. Combination of two components was made without doing any measurements, but with an approximate find of the needed consistency, that is flexible enough, so it can easily fill the sample holder. The mixing was done in a special space behind the glass with a use of medium level ventilation to avoid the possible toxic effects of resin evaporation.

Special sample holders were created and printed by 3D printer from an ABS polymer, in order to fix a fragment of the coin in a needed position inside of another plastic cylindrical sample holder that is directly filled by a resin and keeps the shape. The position of fragments was fixed in a way that would be better for observation of metal alloy, patina formation and corrosion products, after preparation of cross-sections.

The side A and side B of each coin were identified before the resin has covered the sample, since the resin is not completely transparent after it's hardening, that makes identification of obverse and reverse of a coin not anymore possible. That is why the sides were schematically depicted in the notes in order not to lose the information and not to be confused later. Also the point of further cross cutting was defined for each of the mounted coin fragments by measuring the distance between the bottom of sample to the point of cut. For the *Coin_1* and *Coin_4* the distance was 1 cm, for the *Coin_3* it was 7 mm and for *Coin_5* – 1 cm.

Resin samples were left until the next day, since the hardening process of resin takes around 18 hours, and after that the mounted samples were removed from plastic cylindrical sample holders.

The miter saw Micromet Evolution was applied for the second time for performing the next step of cross-sections preparation which was cross-cutting of resin samples. As it was mentioned before, the point where the cross-cutting was defined before mounting the samples, according to the idea of choosing the area in which the all the features of interest would be visible in the cross-section, including corrosion products, metal alloy with its structure, that would be observed with an Optical and Metallographic microscopy.

During the performance of cross-cutting samples were divided in two pieces, each of which was applicable for continuation of cross-sections preparation, but only one was chosen for the further polishing. All samples were cleaned with a use of ultrasonic bath during 15 minutes in a 2-propanol solvent in order to remove the residues of technical oil, that contaminated the samples during their cross-cutting by the miter saw.

- Grinding and Polishing

Polishing was the last and probably the most important part of cross-section sample preparation before starting the microstructural analysis. This process implies smoothing of surface of the cross-cut resin mounted samples of coin fragments by rubbing the surface. The not polished surface of cut resin might look quite smooth, but under the high magnification it appears as rough and looks like 'mountains and hills', what interrupts the procedure of microscopic observation of sample itself. That is why it is necessary to make the surface as smooth as 'mirror' meaning that it should become specular reflective. The process of polishing is quite laborious and requires much time and patience for taking it to an appropriate result.

The polishing was performed with a use of Macatech 24 polishing machine which combines mechanical and chemical forces for better efficiency of smoothing surfaces. If describing simply, the main mechanism of the machine is represented by a retaining disk that rotates with a certain speed while the sample is held against the rotation surface of the disk above it. For the polishing process special abrasive material was used, which is *Struers waterproof silicon carbide paper,* presented in different roughness of grain size - *FEPA #320, 500, 800, 1200 (grain size 15 µm), 2000 (grain size 10 µm), 4000 (grain size 5 µm).* Polishing procedure started with the most rough paper (#320) and consequently graduated to the most fine one (#4000). Paper disk was applied upon the PRESI rotating metal disk. The working conditions were set with a rotating speed of 300 and the time limit of 9000 seconds. The rotation of a polishing disk with a use of silicon carbide papers is usually accompanied with a water supply, in order to increase efficiency of the process.

A sample is held manually towards the mechanical rotation force of the machine, with a control of pressure and friction between silicon carbide paper and the sample surface, that should not be too strong, in order not to destroy the sample, but just to be 'in contact'. The results of polishing action should be checked every several minutes by observing it against the light. When it becomes clearly visible that the grains of abrasive material, depicted on a sample surface as thin lines (polishing relief) that have positions of the same direction, it means that polishing should be stopped with a use of certain paper that should be changed to another paper, which is finer in grain size.

For completing of polishing process and create the final quality of 'mirror-like' surface of resin sample, polishing has been continued with a use of different abrasive material, that provide more gentle abrasive interaction, represented in textile disks with application of diamond pastes, grain roughness of which were *6 µm, 3 µm, 1 µm,*

for increasing the polishing efficiency. They were fixed on the surface of the textile disks, with certain height of fiber applicable for each kind of diamond powder that was mixed with a liquid of Lubricant Reflex LUB. Textile disks were fixed to the polishing machine on a PRESI ceramic rotating disk (instead of metallic one, which was used for silicon carbide papers).

Thus, the polishing procedure is considered to be complete after the application of the finest fibre polishing cloth and diamond paste, resulted in transformation of the resin sample surface to a specular reflective, that would be suitable for performing the microstructural analysis with a use of SEM-EDS, Optical and Metallographic microscopy.

Techniques

- XRD and µXRD

X-ray diffraction technique is a powerful tool for characterisation and understanding of different nature of materials. It is widely applied in study of cultural heritage objects, focusing on specific points as identification and quantification of crystalline compounds and phases, as well as complex polyphase mixtures (applied in study of ceramics, corrosion products, pigments, mortars); the texture of the phases and crystalline orientation (metallographic analysis), and recognition of atomic or molecular structures.

The XRD techniques are based on the phenomenon of diffraction, which occurs when the light sourse radiation whith a certain wavelength is focused on an obstacle with parameters of the same wavelength and magnitude. Atoms have a certain arrangement inside of a crystal unit, organized by distances between atoms and their directions (defined by crystalline planes). Since crystal have diffraction gratings for X-rays, they scatter X-rays in an order that shows atomic positions inside a crystal grid. Consequently, diffraction obtained from different planes of atom gives a diffraction pattern which contain information about all the arrangements inside of a crystal. In order to define a crystalline compound, such parameters as intensity, width, position and shape of the peaks of the diffraction pattern. For successful results of XRD analysis the Bragg's law should be satisfied, managing the settings of analysis before starting it: the X-ray wavelength should be fixed, as well as a specific angle, at which the planes produce a diffraction pattern. The interpretation of results is based on a space between diffraction planes of atom that determines the peak position, and the peak intensity that determines what the atoms of those diffraction planes are.

Micro X-ray diffraction (µXRD) allows examination of very small areas of a sample, focusing the incident beam on a certain spot (several micrometres) on a sample surface, providing the knowledge of crystalline structure of material. The conventional XRD instrument is more bulky and it has a high power requirements, while the intensity of a µXRD beam can be reached in a lower power source.

The micro X-ray diffraction analysis was performed in DISAT laboratory of Politecnico di Torino with a µXRD Rigaku Rint/Rapid.

- Metallography

Metallography is a scientific study of metal alloy characteristic and identification of it's chemical and atomic microstructure and composition, spatial distribution of it's constituents, determination of alloy phases. Metallographic phases are the homogenous parts of the material, consisted of the solvent and solute, that have different composition and properties. In case of the presented bronze coins the solvent is copper and the solute is tin. Also, metallography is useful for observing various inclusions within an alloy, crystallographic texture and matrix observation, examination of chemical and electrochemical surface changes like corrosion, oxidation and contamination, determination of mechanical and thermal processing, defects analysis (porosity and cracking). In this technique, the sample preparation requires fine polishing and chemical etching, which applied in order to

reveal the microstructure and its features. The sample preparation concerning the current thesis work is described in details below.

In a field of cultural heritage diagnostics, particularly in case of metal objects studies, the metallography is applied in order to find out what changes the metals face during their existence, and understand the microstructure transformations due the metal production processes and its solidification, considering the manufacturing conditions and methods in ancient times. 'The main disadvantages are invasiveness of the measurement, and the fact that only a small two-dimensional section of the object is analysed, so that the results lack statistical significance and do not capture the three-dimensional nature of the material. Furthermore the characterisation of the exact composition of the metal phases requires complementary point or bulk chemical analysis for the complete interpretation of the artefact [17][3].

The metallographic analysis is usually performed with a Brightfield illumination optical microscope. 'In incident BF, the light path comes from the light source, passes through the objective lens, is reflected off the surface of the specimen, returns through the objective, and finally reaches the eyepiece or camera for observation. Flat surfaces produce a bright background due to reflection of a large amount of the incident light into the objective lens, while non-flat features, such as cracks, pores, etched grain boundaries or features with distinct reflectivity, such as precipitate and second phase inclusions on the surface appear darker as incident light is scattered and reflected at a variety of angles or even partially absorbed' [18].

During the experimental work for this thesis research, the metallographic microscopy was carried out with a Brightfield illumination optical microscope Leica (of the Politecnico di Torino DISAT laboratory) which has a range of magnification of 50, 100, 200, 500, 1000 and 2000X.

The method of etching was applied for the efficiency of metallographic analysis. Etching is used in metallography in order to reveal some details that cannot be visible as-polished. It is possible to observe without using the etching certain kinds of defects, like cracks, inclusions and porosity. However, only the etching procedure makes able to identify such details of metal microstructure as grain size, their borders and distribution, phases distribution, dendrites or other kinds of alloy microstructure.

Two etchants were chosen for the metallographic attack. The first (etching solution № 1,Table 1) etchant consisted of ammonium hydroxide (NH_4OH), hydrogen peroxide (H_2O_2) and distilled water (H_2O) in proportions showed in a following table. The second (Etching solution № 2, table 2) was composed of Ferric chloride ($FeCl_3$), hydrochloric acid (HCl) and distilled water (H_2O).

Samples of coins in cross sections mounted in a resin were prepared for the metallographic analysis by grinding and polishing the surface until it acquired the specular reflectance appearance, as it was described previously.

---

[17] [3] G. Artioli, *Scientific Methods and Cultural Heritage: An Introduction to the Application of Materials Science to Archaeometry and Conservation Science*, vol. 9780199548. 2010.

[18] Dionis Diez. Metallography – an Introduction. How to reveal microstructural features of metals and alloys. http://www.leica-microsystems.com/science-lab/metallography-an-introduction/

Etching was performed between the microscopic observations several times. The etching solution was applied on a surface of sample and kept for controlled certain amount of time (minimum 10 seconds). The time of etching and the quantity of procedures defined experimentally, depended on the results gained after each of the etching procedure, that are described bellow.

Table 2. The etching solution № 1 composition

Composition	Proportions (ml)
NH_4OH	10
H_2O_2	15,4
H_2O	0,6

Table 3. The etching solution № 2 composition

Composition	Proportions
HCl	15 ml
H_2O	60 ml
$FeCl_3$	5 g

- SEM-EDS

Scanning electron microscopy coupled with Energy dispersive X-ray spectrometer is one of the most effective archaeometry techniques of high accuracy and precision, which is indispensable for observation and identification of wide range of materials, and for qualitative and quantitative analysis of other different material and for surface morphology. The principle of technique is based on a contact between an electron beam and the surface of a sample. The primary electron beam scans the surface sample, and depending on the material analysed and also on set of acceleration voltage, secondary signal is generated in an interaction volume and it is used in creation of images and analysis. The secondary products that are most common used for images creating are secondary electrons (SE) and Backscattered electrons (BSE). Secondary electrons signal appears in result of inelastic scattering of primary electrons on an atomic core of the sample material. Secondary electrons are low in energy (less than 50 eV). The contrast of the image created with secondary electrons depends on the morphology of a sample, increasing the topography visible features. Backscattered electrons are those with energy higher than 50 kV, generated by elastic scattering on a deeper level of interaction with sample material. BSE images are usually high in contrast, which depends on a chemical composition of a sample. In order to obtain high quality imaging of sample, it is better to apply lower acceleration energy of primary electrons, for smaller penetration depth and interaction volume. In that case, secondary electrons contact the upper layers of sample material and create an image of better contrast with a more clear visibility of surface structure.

EDS is a microanalysis technique that works in combination with SEM for a identification of elemental composition and quantification of elements. EDS is able to detect the X-rays reflected from the sample during its bombarding by an electron beam for acquiring the characteristic information about the elemental composition of analysed area of a sample. It can be focused on a small areas, even less than 1 µm.

The analysis of Roman coins were carried out by Scanning Electron Microscope Zeiss Supra 40 (DISAT laboratory of Politecnico di Torino), supplied by Gemini detector, Field Emission electron source and with a focused electron beam create high resolution images of a surface and provide information about topography and elemental composition.

In order to perform analysis with accurate results by means of SEM-EDS, the samples had to be prepared in a certain way.

The resin mounted samples were attached to a SEM metallic sample holder in a way to create further good conduction between SEM electrons and a sample surface. Sample was attached upon a carbon tape and a drop of silver glue between back side of the sample and metal surface of a sample holder. Another small drop of conductive silver glue was applied on the edge of specimen and after a tiny 'bridge' of silver glue was made on a resin surface, connecting the specimen and the metal of sample holder.

Each sample was placed into the oven for 2 hours with a temperature of 40 ^{0}C in order to liquidate the resin gases as much as possible, so they would not make a contamination inside of a SEM-EDS chamber, interrupting the contact between electrons and the sample itself.

After heating procedure samples were placed into the vacuum chamber (?) for several days before the analysis with SEM-EDS.

It is necessary to put in evidence that samples were not subjected to any metallisation coating that is usually performed before SEM-EDS analysis, in order to increase conductivity of specimen and electrons inside of instrument chamber. It was impossible to use carbon coating because of extra high vacuum conditions and sensitivity of instrumentation.

The variant of golden sample coating was not applicable due to elemental coincidence with specimens. The energy of characteristic X-rays of lead (Pb Lα – 10.550) is similar to the X-ray energy of gold (Au Lα – 9.712), which could potentially make a confusion during the EDS detection, because lead is presented in samples in high quantity.

The sample coating with chromium was considered as possible in case of high necessity, though the methodological aim of analysis was pointed on obtaining the accurate analysis results without an application of any conductive coating for samples except of the conductive silver 'bridge'.

However, several difficulties appeared analysing uncoated samples with SEM-EDS. Firstly, it was possible to observe the sample only in areas near to silver 'bridge', which provides better conductivity and less loss of electron counts. Secondly, the resin gases evaporation affect the vacuum system, and it requires more time than usual to reach the necessary vacuum conditions. In order to avoid those problems, samples were always placed into the vacuum chamber for several days before performing the SEM-EDS analysis.

Also, during the EDS mapping process the resin interrupts and reduce the electrons current focusing, that creates distortion and shifting of mapping imaging,

The mapping of alloy phases of the bronze Coin_1 sample was performed in DISAT laboratory of Politecnico di Torino with Zeiss Merlin Scanning Electron Microscope with a Gemini II optical column, 3D surface topography visualisation system, Inlens Secondary Electrons detector for providing images of high resolution and Energy selective Backscattered detector for a material contrast (and also Angle selective Backscattered detector for analysis of surface crystalline contrast structure).

- XRF

X-ray fluorescence is an extremely useful tool in application to Cultural Heritage objects analysis to recognize and analyse different inorganic materials as metals, pigments, glasses. This technique is appreciated for its high sensitivity, rapidity and non-invasiveness for the artefacts, analysed for detection of elemental composition, qualitative and quantitative bulk analysis of major and trace elements. Moreover, this technique is usually represented in a portable construction that allows the analysis performance in-situ. In case of this study, the typical for ancient bronze elements were expected to be detected in a bulk alloy, such as copper, lead, tin, zinc, but it is also important to define their correlation. The analysis of surface of coins was performed in order to detect elements that are related to the corrosion presence and environmental conditions that the objects faced during their burial.

XRF principle is based on the emission of secondary or characteristic electrons (photons) from a material that was bombarded by a high energy X-rays (primary radiation). 'The energy of the emitted photon will be equal to the difference in energies between the two orbitals occupied by the electron making the transition. Because the energy difference between two specific orbital shells, in a given element, is always the same (i.e. characteristic of a particular element), the photon emitted when an electron moves between these two levels, will always have the same energy. Therefore, by determining the energy (wavelength) of the X-ray light (photon) emitted by a particular element, it is possible to determine the identity of that element' [19].

In case of ancient coins examination, XRF is not surely reliable in quantitative analysis, because of the low energies of primary radiation, that does not penetrate the sample deep enough to obtain an accurate data. For that reason, the XRF results need to be correlated with results from other techniques, like SEM-EDS which is more powerful in this particular field of application.

The analysis was performed with a help of Prof. Stefano Ridolfi and Ars Mensurae, the laboratory of diagnostics in Cultural Heritage (Rome). The equipment used for the characterization of Roman bronze coins is a portable Amptek X-123SDD X-R ay Spectrometer with a double laser point system and Silicon Drift Detector (SDD)

[19] XRF principles. Basic theory. http://learnxrf.com/

coupled with a Mini-X X-Ray Tube System equipped with a Tungsten golden anode (50 kV/35 μA). System is supplied with three batteries.

In order to obtain accurate results of chemical characterisation, the patina layer was removed with a polisher, revealing the area of bulk metal on a coin, with a size of approximately 5 mm. Samples were placed in a 2 cm distance from the tube and detector, the two lasers were pointed manually towards specific points that are referenced with numbers and pictures.

All the measurements were done with fixed instrumental conditions: 38 kV of applied high voltage and 15 μA of cathode current, with 80 seconds time of analysis. Data acquisition was performed through a PC card (DPPMCA software).

Results and discussion

Bulk alloy analysis

Coin_1

Figure 21. Coin_1, SEM-EDS image of an area with 2 alloy phases

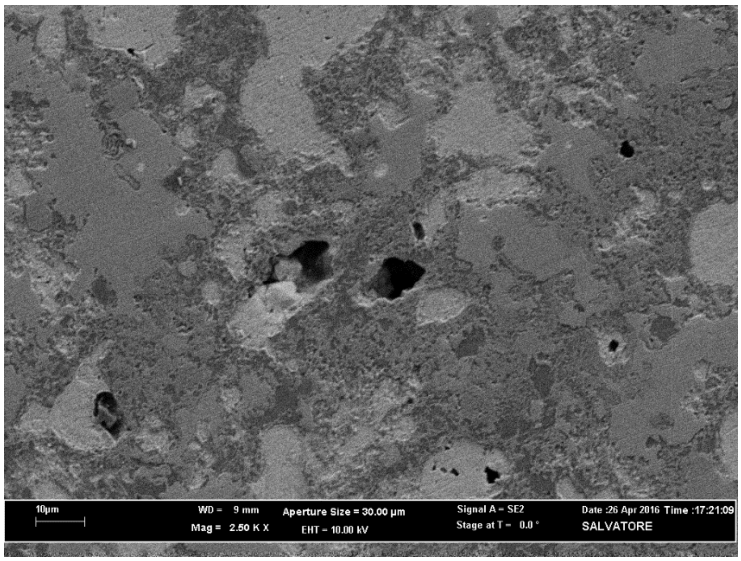

The image of Figure 21 was taken with a secondary electrons detector, with conditions of working distance – 9mm, current energy 10.00 kV, aperture size 30.00 µm and magnification of x2500. The chosen area shows the phase of Cu-Sn bronze as one phase of alloy, represented in darker colours on the image, and a distribution of lead particles as another alloy phase, seen in lighter coloured spots.

Figure 22. EDS images of spot analysis areas (a,b).

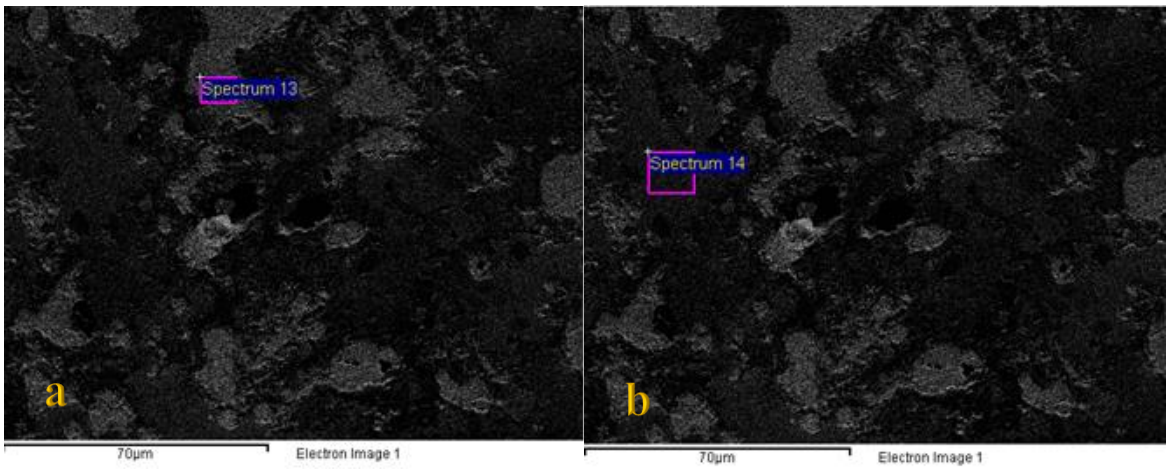

Figure 22 (images **a** and **b**) EDS imaging shows spot analysis areas. Area of lead particle (light grey spot) is shown on image **a**, image **b** shows a spot of bronze alloy phase (dark grey).

The elemental composition is provided in the following spectrums (Figure 23 and Figure 24):

Figure 23. Coin_1, EDS spectrum of a bronze phase spot of analysis.

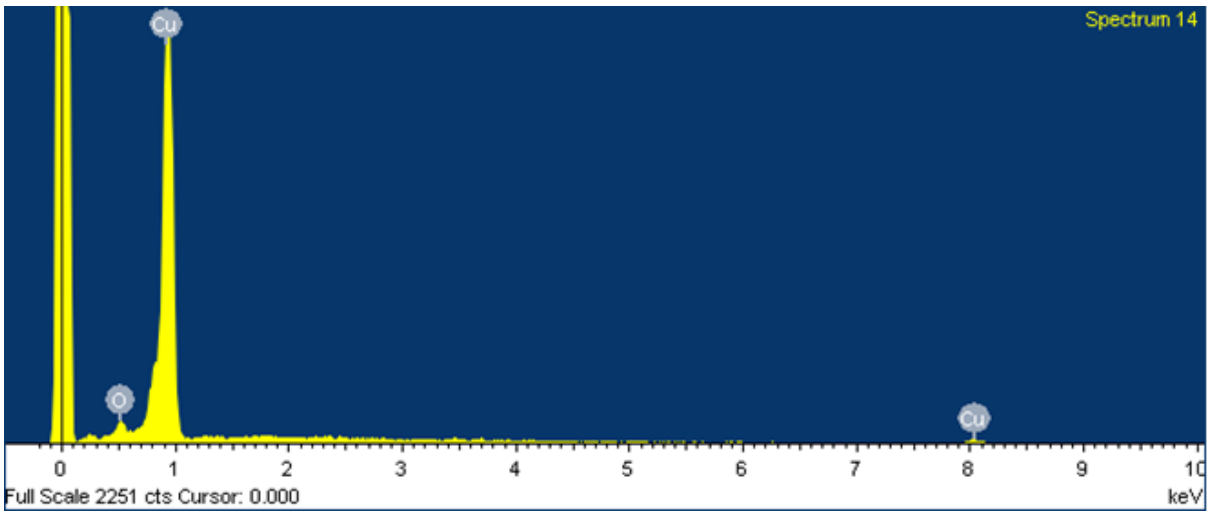

Figure 24. Coin_1, EDS spectrum of a lead phase spot of analysis.

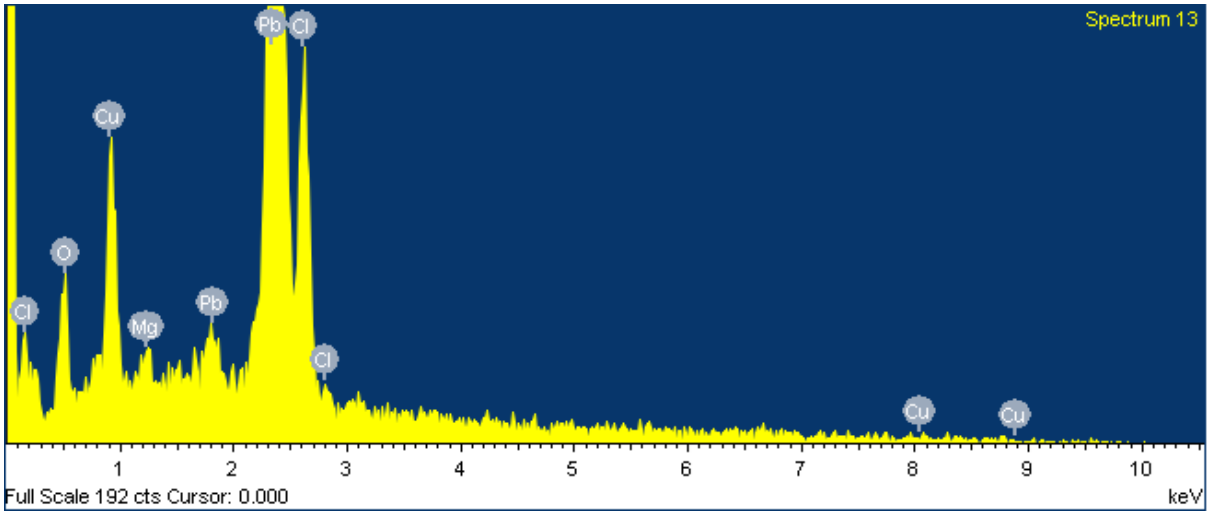

Spectrum of Figure 24 is related to a spot of lead particle as a separate phase in a coin alloy (Image **a**, Figure 22), thus Pb is prevailing element in the spectrum. Chlorine, probably chlorine oxides and lead chlorite and magnesium are presented because of the corrosion products formed close to lead particles distributed in the alloy. Copper is also detected at this spot as the bronze phase component.

Elemental composition detected from another analysis spot (Image **b**, Figure 22) consist mainly of copper, however tin has not been detected here as the solute of bronze phase.

Figure 25. Coin_1. SEM-EDS secondary electron images of analysed area of bronze phase

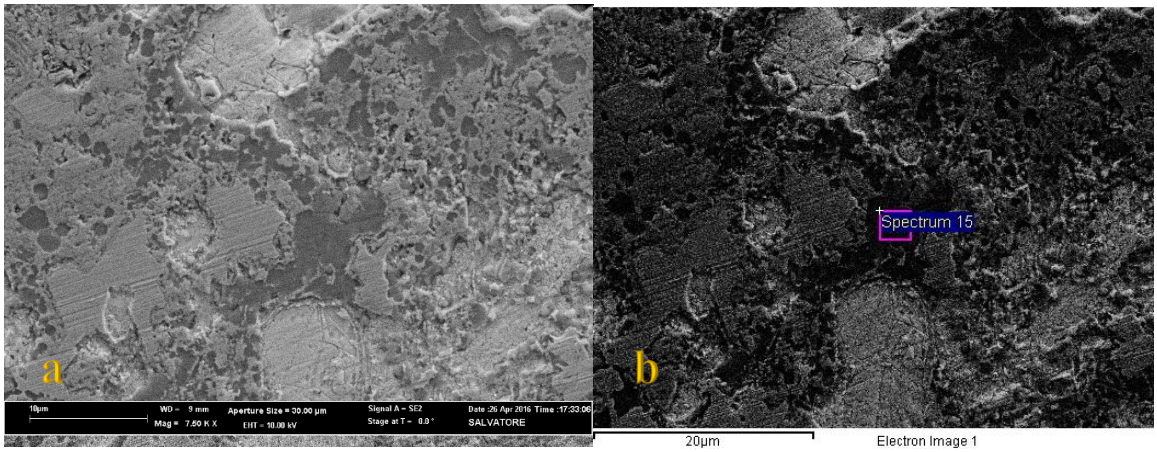

Figure 25 represents a secondary electrons SEM-EDS image of a bronze phase area spot composition analysis, which appears on a picture in area of a dark grey colour. Image **a** was made with a less current energy (10.00 kV) for a better imaging quality, instead of image **b** which was made during the EDS spot analysis with higher current energy of 15.00 kV.

Figure 26. Coin_1, SEM-EDS spectrum of the bronze spot (Figure 4).

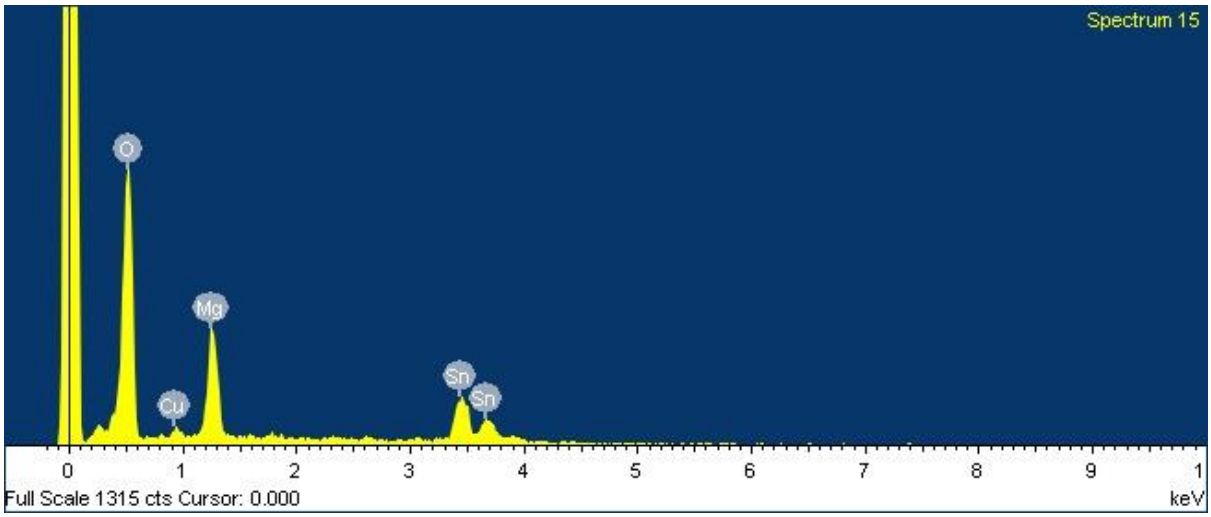

The compositional spectrum (Figure 26) reveals elements related to a bronze phase – copper and tin, where tin has a prevailing amount in this particular spot. The detection of high level of magnesium is probably due to the corrosion products presence.

The mapping of alloy phases of the bronze Coin_1 sample was performed with Zeiss Merlin Scanning Electron Microscope with a Gemini II optical column, 3D surface topography visualisation system, Inlens Secondary Electrons detector for providing images of high resolution and Energy selective Backscattere detector for a material contrast (and also Angle selective Backscattered detector for analysis of surface crystalline contrast structure).

Analysis was done in order to have an idea of elements distribution in a particular area of interest, which is indicated in a following image:

Figure 27. Coin_1, SEM-EDS backscattered electrons image.

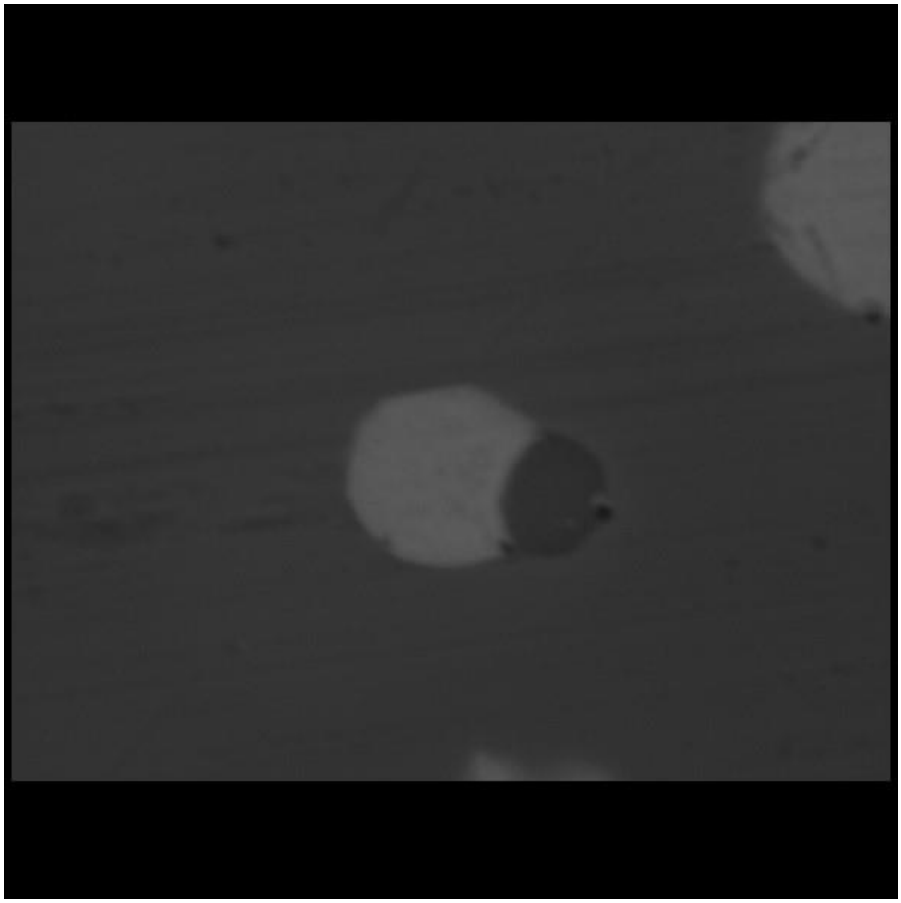

Figure 27 represents a particle of lead inside of a copper-tin alloy.

Figure 28. SEM-EDS mapping of 3 elements (Cu, Pb, Sn) in particular.

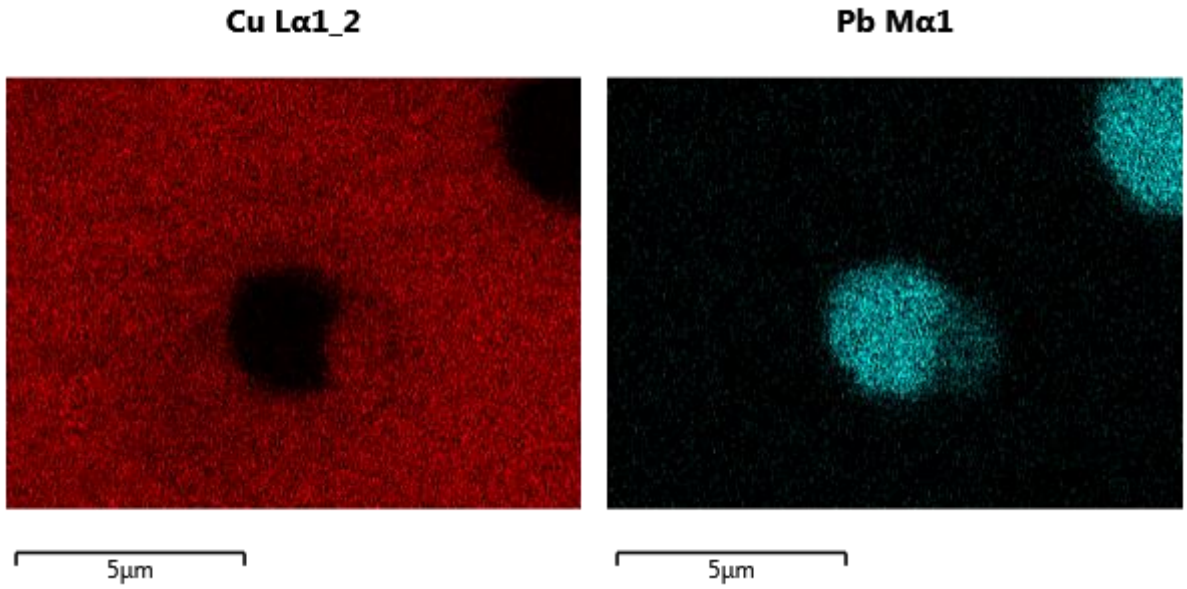

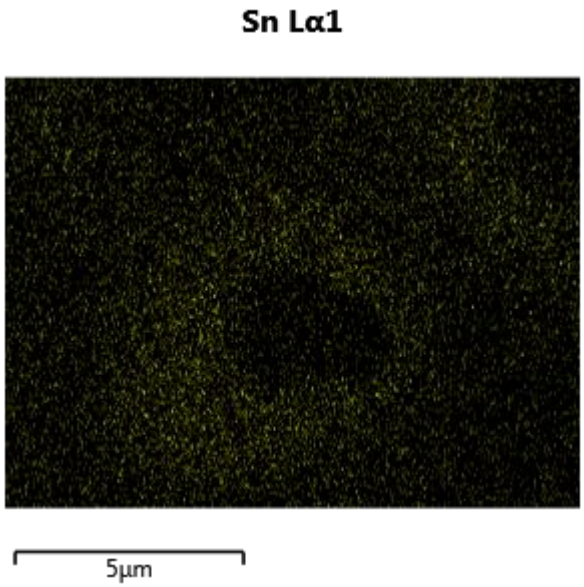

Figure 28 represents mapping of three elements (copper, lead and tin), their particular distribution within a chosen area, the same as on a Figure 27.

Figure 29 shows the elemental mapping of the chosen area. The blue area represents the particle of lead, which is located within the copper-tin phase (Cu assigned as red and Sn – yellow). At the same time there is another phase of copper and lead pointed on the picture as Pb-Cu phase.

Figure 29. Coin_1 SEM-EDS mapping

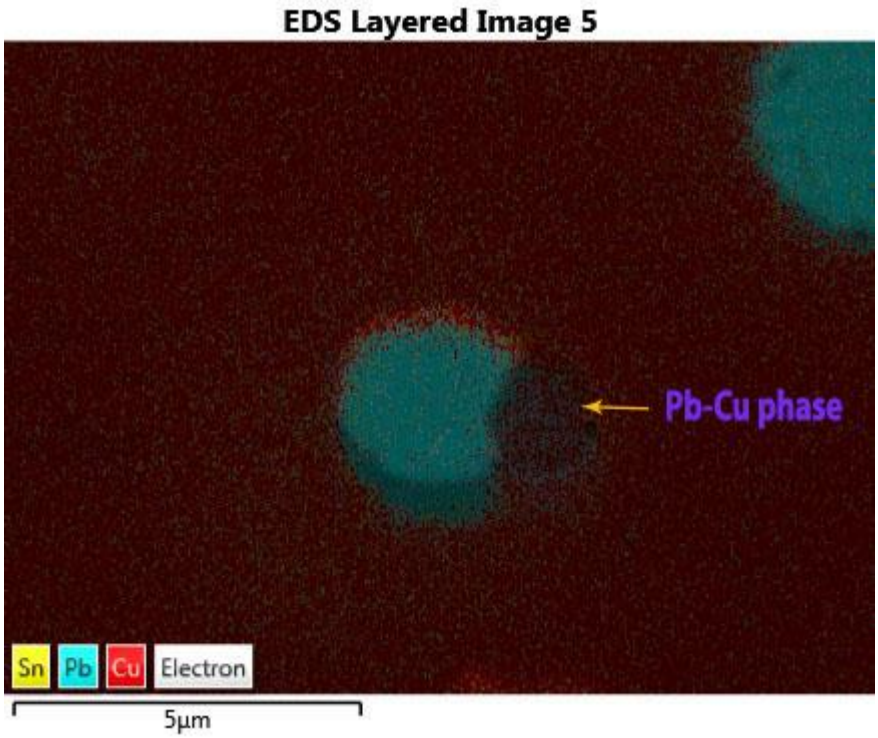

The XRF analysis of bulk alloy of Coin_1 provided information on elemental composition, according to interpretation of XRF spectrum peaks (shown on the spectrum of Figure 30): The most intensive peaks are related to presence of copper (energy level of Kα is 8.05 kV and Kβ – 8.86 kV) and lead (Lα - 10.55, Lβ - 12.61 kV). The minor element is tin (Kα – 25.27 kV, Kβ – 28.48 kV).

Figure 30. Coin_1 bulk alloy XRF spectrum.

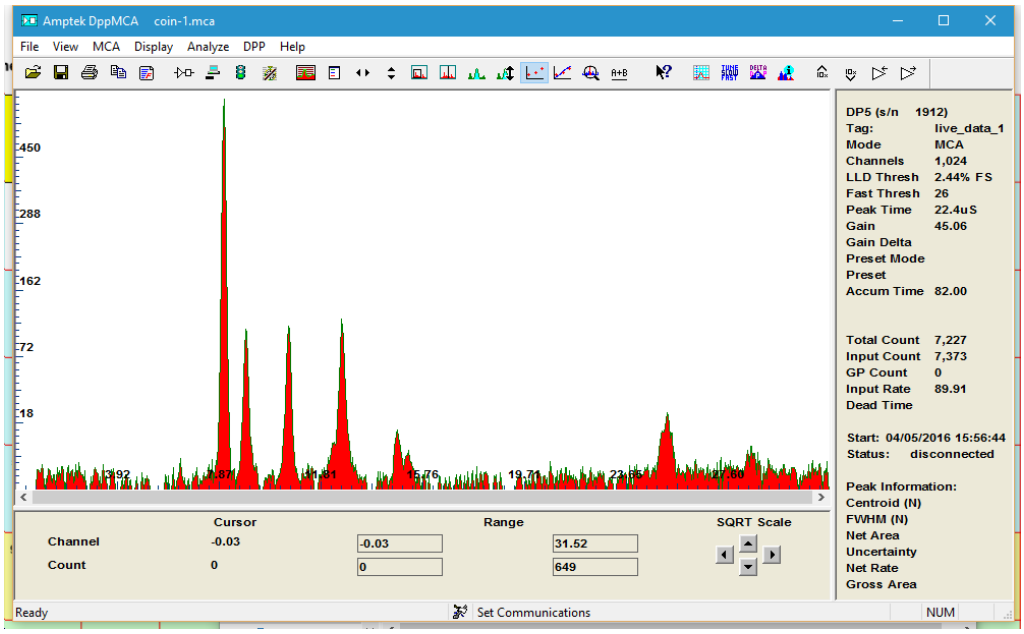

Coin_3

Metallographic phases of the Coin_3 sample were examined with FESEM Scanning Electron Microscope.

Figure 31. Coin_3, SEM-EDS backscattered (a) and secondary electrons (b) imaging.

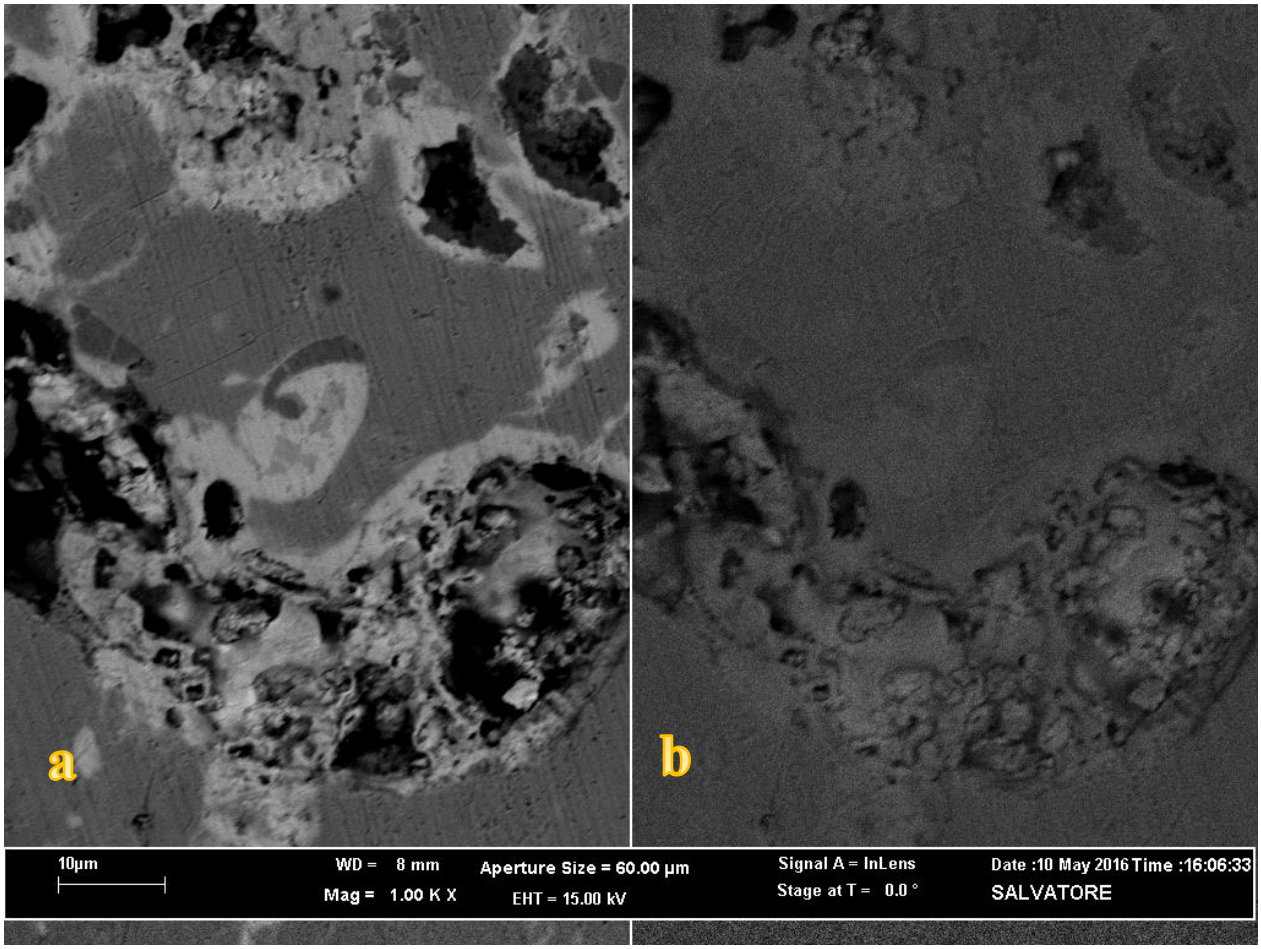

The area on the image of Figure 31, chosen for the SEM-EDS imaging and compositional analysis includes several phases of alloy, formed during the casting of the coin. The image was made with application of the two detectors (backscattered and secondary electrons) at the same time, with magnification of x1000, working distance of 8 mm, aperture size of 60.00 µm and current energy of 15.00 kV. Image **a** was generated by backscattered electrons and the contrast is managed according to an elemental composition diversity. The contrast imaging features of the **b** image are based on the topography of the sample surface.

Figure 32 represents four backscattered images of different EDS analysis spots (a, b, c, d) at an area that includes several metallographic phases. The following spectrums show the elemental composition of every spot.

Figure 32. Coin_3, SEM-EDS backscattered electrons images of different spots of analysis (a, b, c, d).

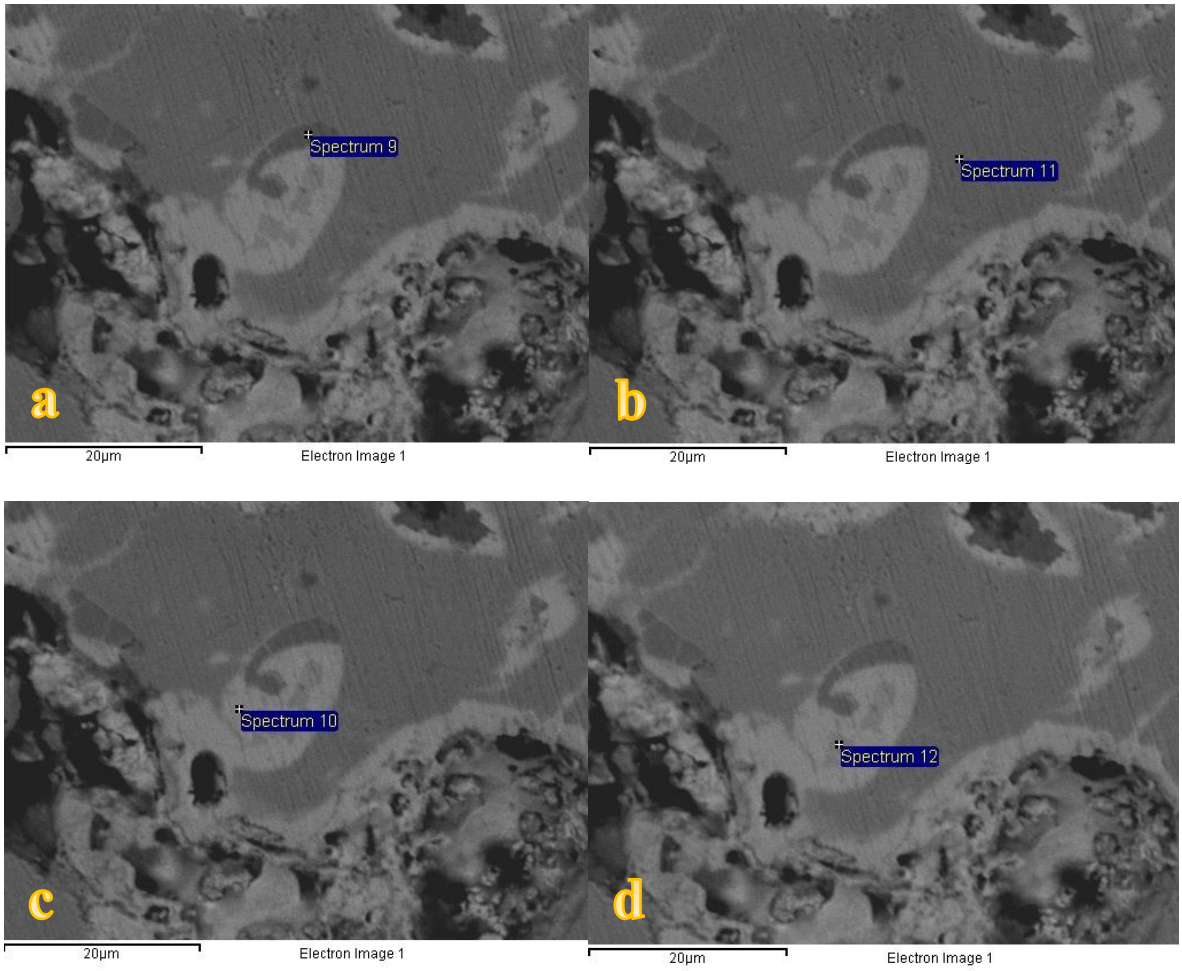

Figure 33. Coin_3, EDS spectrum of a spot of image a (Figure 32)

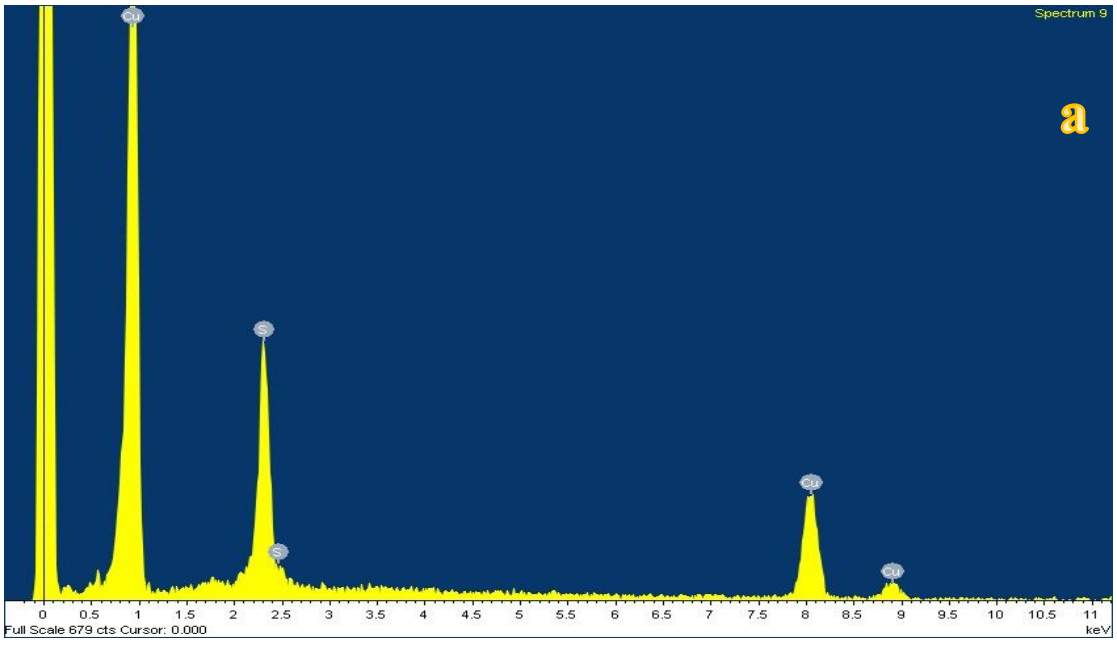

Figure 34. Coin_3, EDS spectrum of a spot of bronze phase (image b, Figure 32)

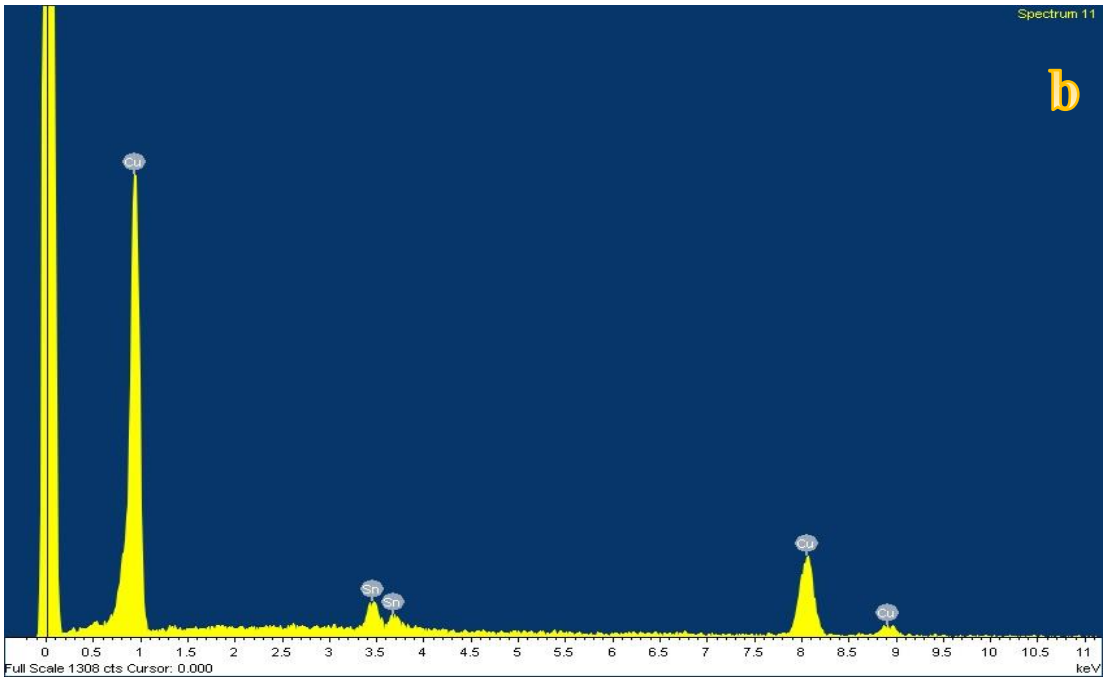

The presence of sulphur, which was detected besides of copper in a point of image **a** (Figure 32) and showed by relevant spectrum on Figure 33, can be possibly related to corrosion products.

The spectrum of Figure 34 represents the elemental composition of a solid bronze phase captured by EDS analysis spot (image **b**, Fugure 32), which consist of copper as a solvent and tin as a solute.

Figure 35. Coin_3, EDS spectrum of a spot of image c (Figure 32)

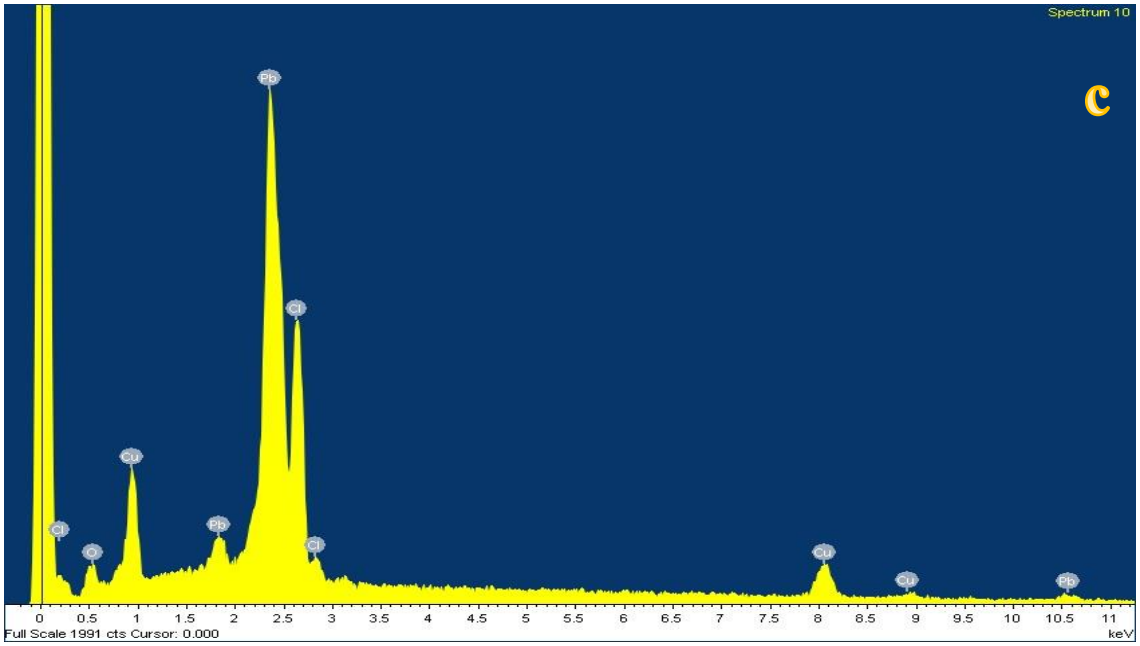

Figure 36. Coin_3, EDS spectrum of a spot d (Figure 32).

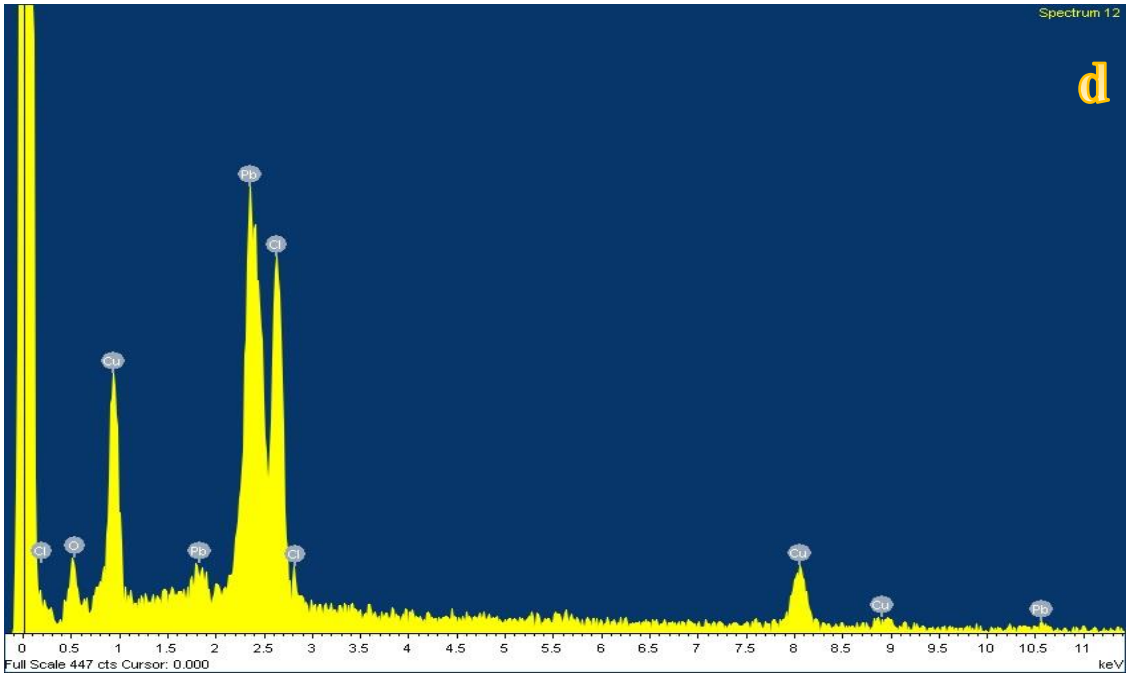

Spectrums of Figure 35 and Figure 36 relevant to analysis of spots **c** and **d** (Figure 32) show the same elemental content, but with difference in peaks intensity which related to a quantitative distribution of elements. The amount of lead is higher in the spot **c**, and lower in the spot **d**, while copper and chlorine are relatively lower in the spot **c** and decrease in the spot **d** spectrum. Chlorine and oxygen are presented possibly due to corrosion formation that usually forms nearby lead inclusions in an alloy. Both spots **c** and **d** probably belong to a particular phase of copper and lead, and the occurrence of this phase is also identified in other coins' samples (Coin_1 and Coin_4).

Figure 37. Coin_3 bulk alloy XRF spectrum.

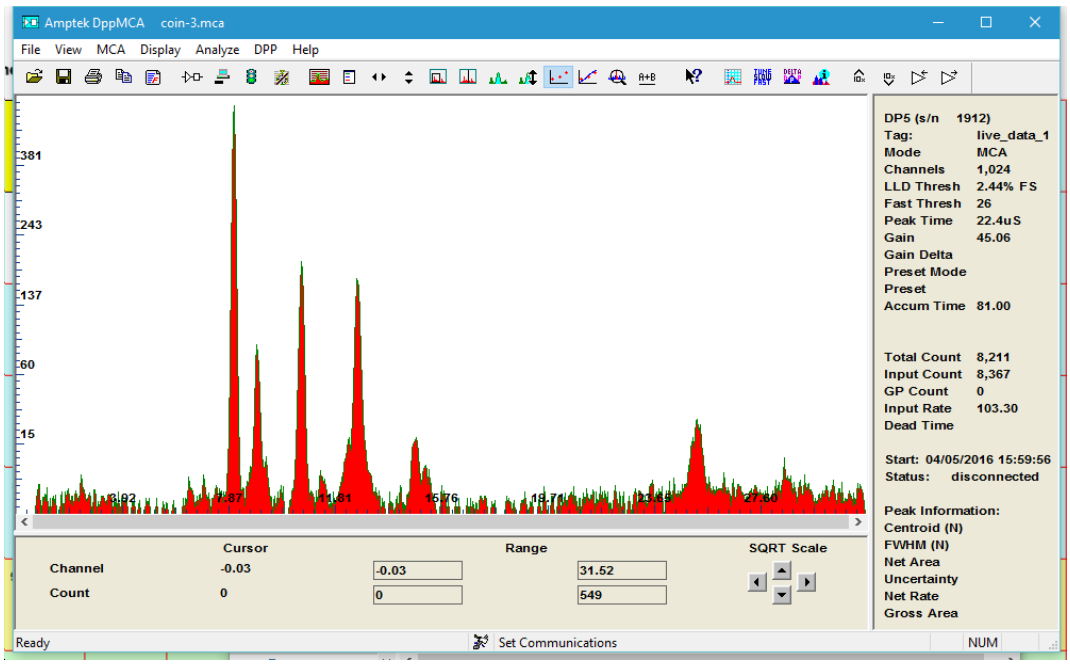

XRF analysis results of Coin_3 bulk alloy revealed the elemental composition where the major element is copper, level of lead in the alloy is high (around 40%) and tin is another element of bronze composition. Peaks of iron (Kα 6.40 kV, Kβ 7.06 kV) are presented due to pollution from the environment. The peak of cobalt appears in the spectrum (Kα 6.93 kV), that can refer to possible painting of coins with a blue cobalt pigment (Figure 37).

Coin_4

The elemental compositions of alloy phases of sample Coin_4 were examined with SEM-EDS analysis.

Figure 38. Coin_4, SEM-EDS image of the spot analysis of bronze phase

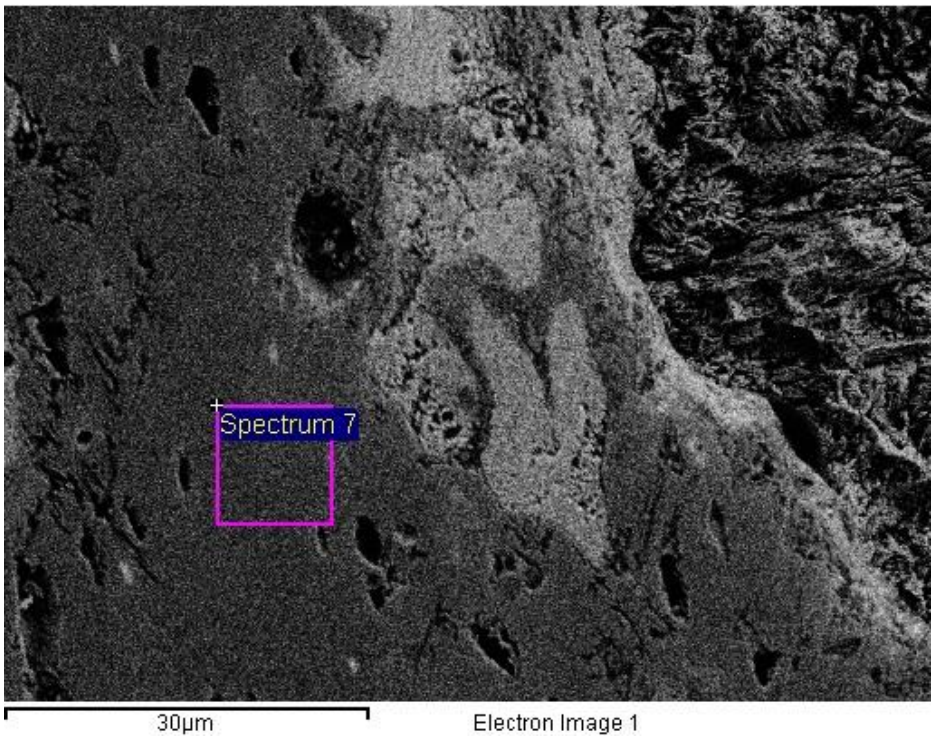

Figure 39. Coin_4, SEM-EDS image of the spot analysis of lead phase

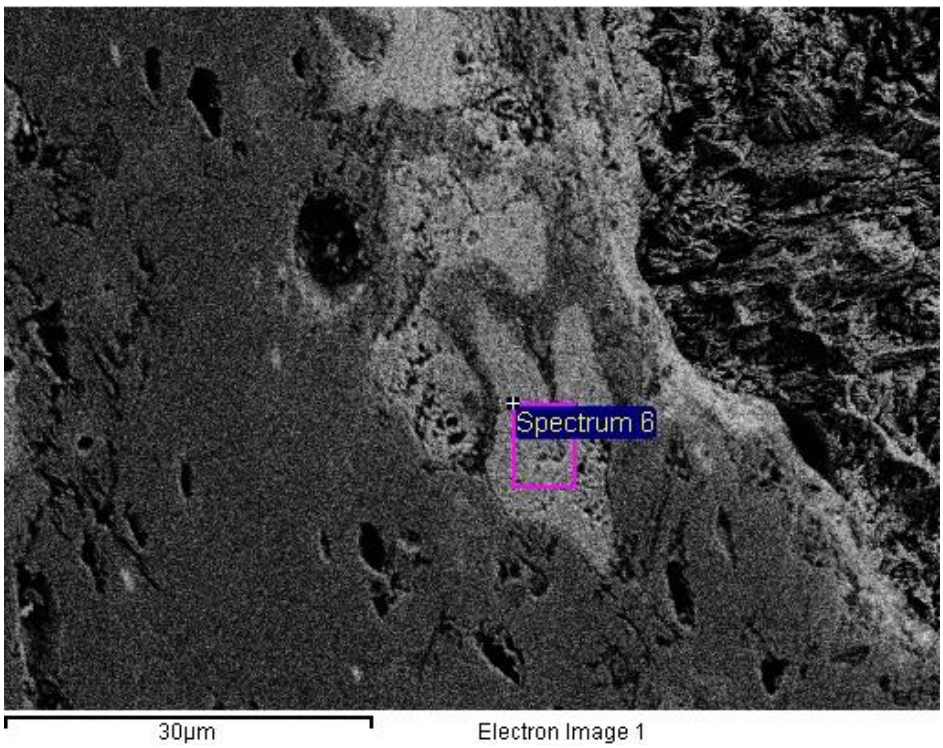

The area with 2 spots of analysis, indicated on Figure 38 and Figure 39, was analysed with a secondary electron detector, in conditions of 4 mm of working distance, current energy 10.00 kV, magnification of x 2500 and aperture size of 30.00 µm.

The first spot, shown by Figure 38 in a dark grey colour, captures the bronze phase of the alloy, the composition of which is presented in a following spectrum (Figure 40) and proves that the bronze phase consists of elements of copper and tin with a prevailing amount of copper as a solvent.

Figure 40. Coin_4, SEM-EDS elemental composition spectrum of bronze area of spot analysis

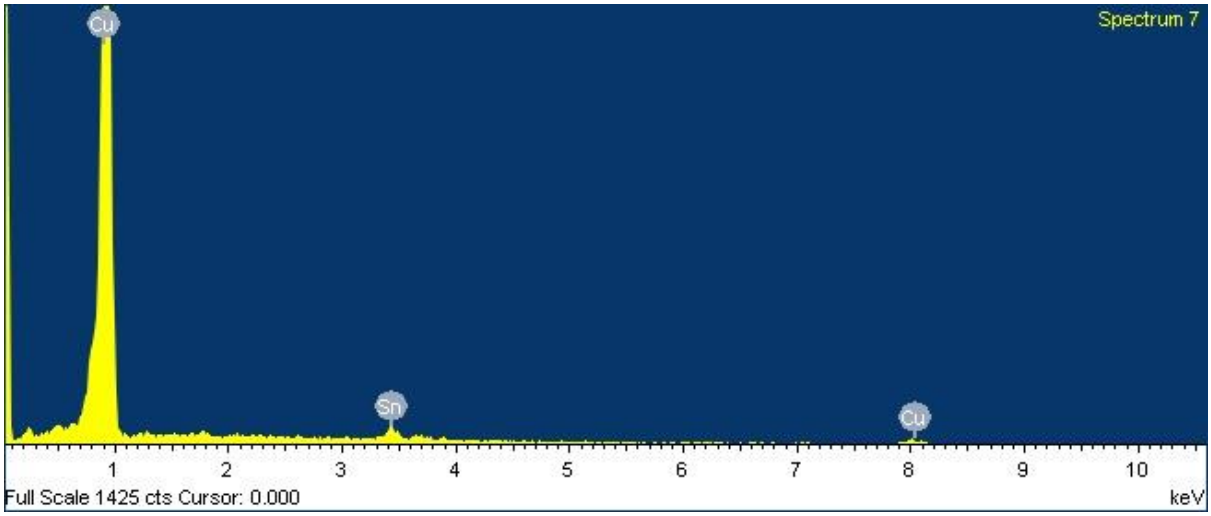

Figure 41. Coin_4, SEM-EDS elemental composition spectrum of lead particle area of spot analysis

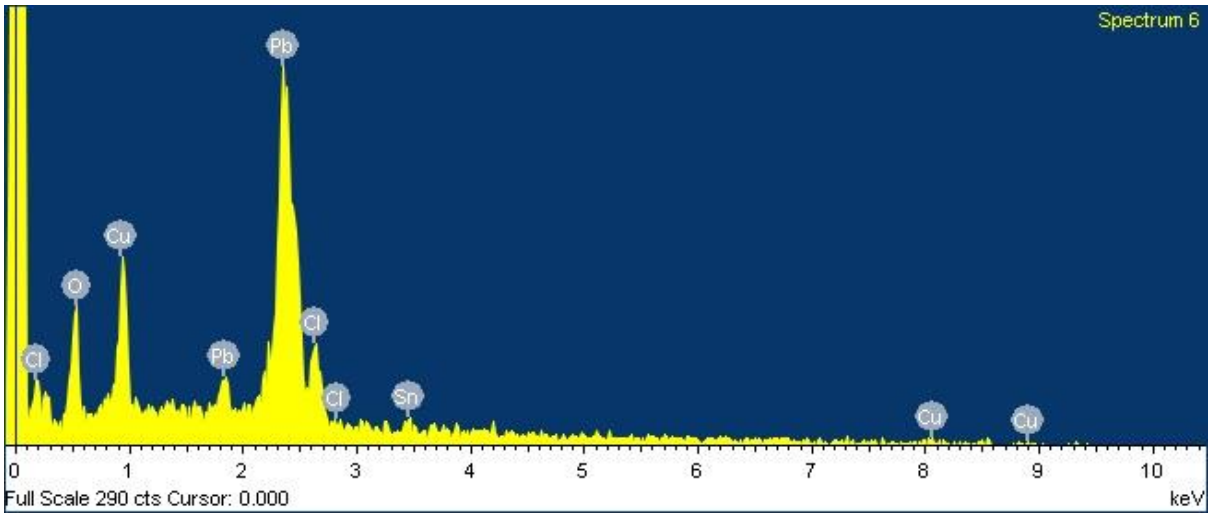

The elemental spectrum of another spot of analysis (indicated by Figure 39 in light grey colour) is shown on a Figure 41. Lead is presented in a highest amount, which indicates that the analysed spot belongs to a phase of lead, that distributed within the bronze phase of alloy.

The presence of copper and tin elements is detected probably because the spot was captured not exactly and only on a lead particle. The chlorine oxides are related to corrosion products occurred in the area of analysis, since corrosion is very sensitive to lead.

Figure 42. Coin_4, SEM-EDS image, backscattered (a) and secondary electrons (b) imaging.

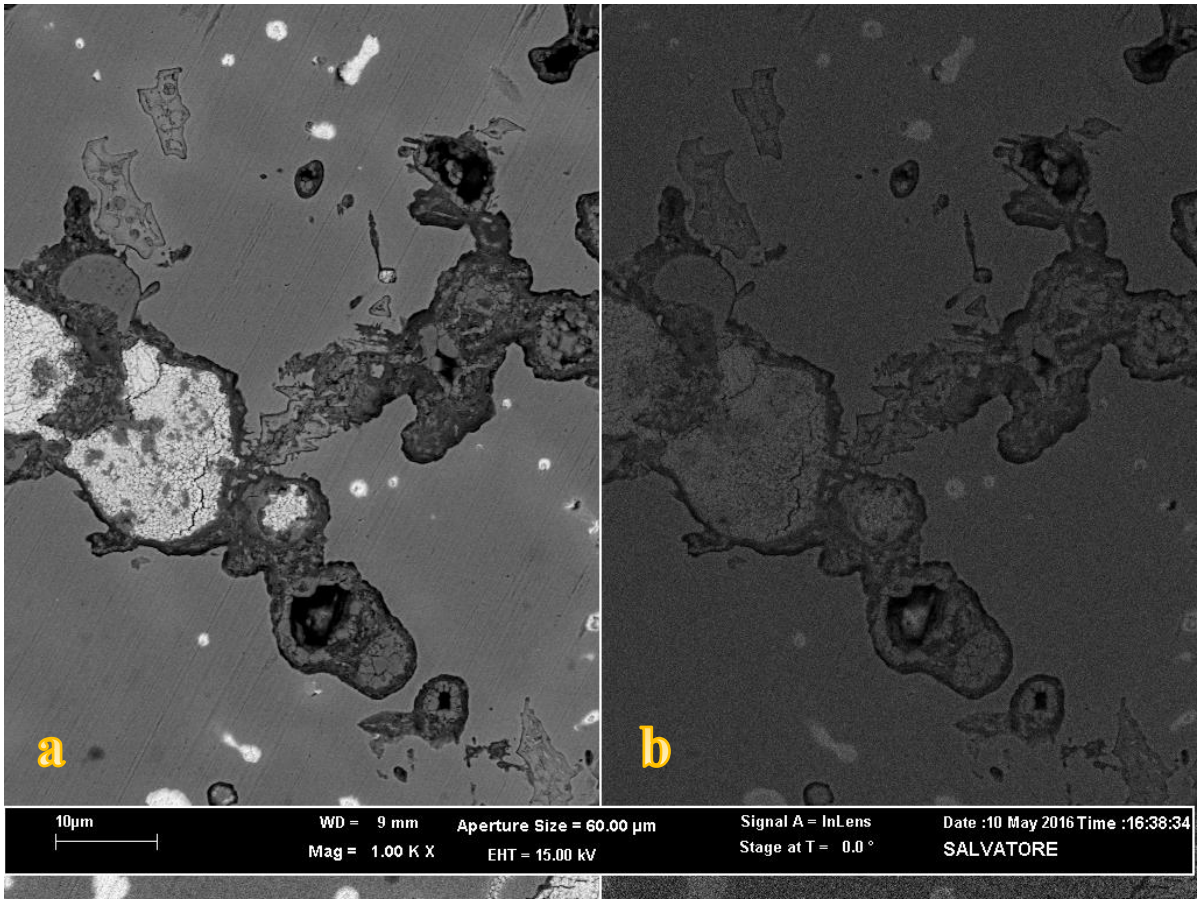

Figure 42 represents an image of an area of bronze matrix with inclusions of lead and corrosion products formed near to lead particles. The imaging was made with use of two detectors at the same time: backscattered electrons detector (image **a**) and secondary electrons detector (image **b**). Backscattered electrons are those with energy higher than 50 kV, generated by elastic scattering on a deeper level of interaction with sample material. BSE images are usually high in contrast, which depends on a chemical composition of a sample. Secondary electrons signal appears in result of inelastic scattering of primary electrons on an atomic core of the sample material. Secondary electrons are low in energy (less than 50 eV). The contrast of the image created with secondary electrons depends on the morphology of a sample, increasing the topography visible features. However, the image of Figure 43 was made with a 15.00 kV energy of primary electrons current, magnification of x1000, aperture size of 60.00 µm and a working distance of 9 mm.

Figure 43 is an image of a lead inclusion (light grey area) from the same area of analysis (Figure 42) with a highlighted spot of spectrum requirement.

Figure 43. Coin_4, SEM-EDS backscattered electrons image of a lead particle

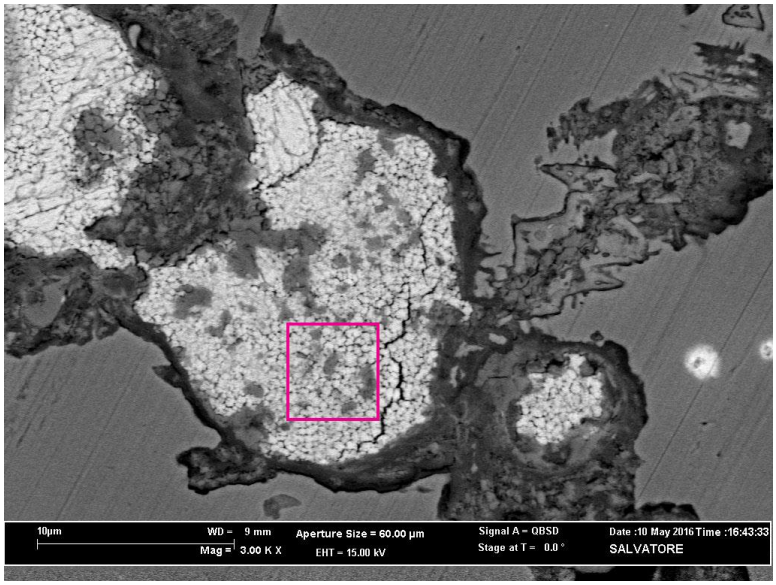

Figure 44. Coin_4, EDS spectrum of a lead spot (Figure 43)

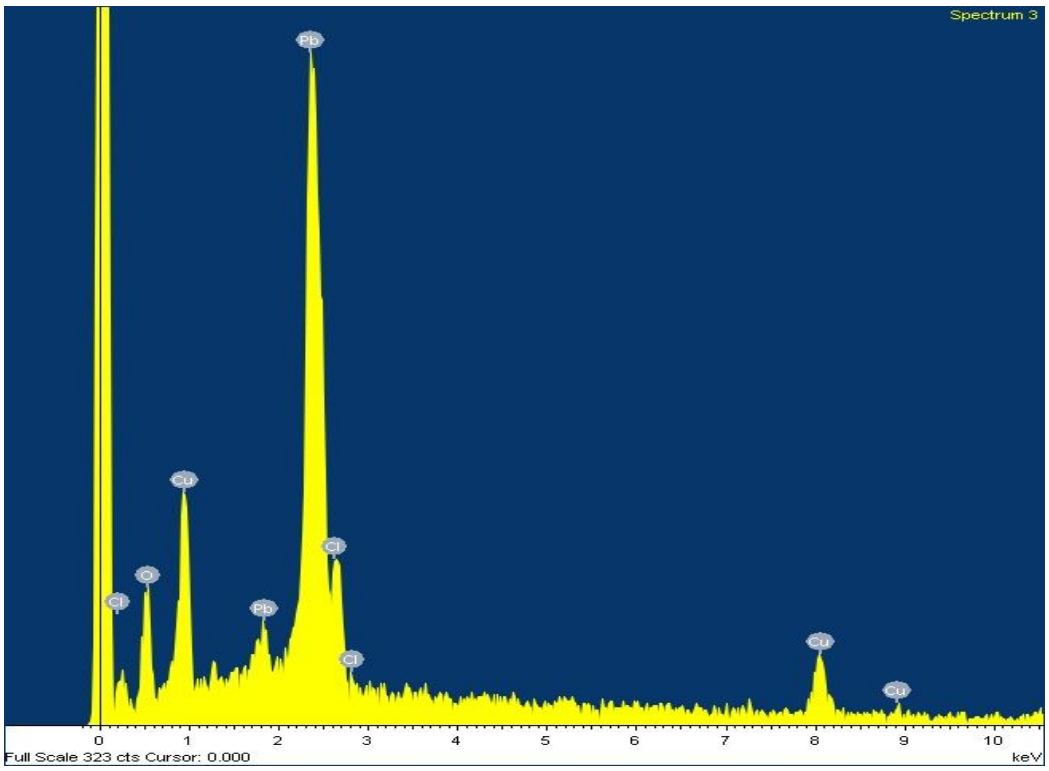

Compositional EDS spectrum shown by Figure 44 reveals the range of elements presented in this particular spot. Lead appears in a highest amount. Elements of copper and chlorine are most probably related to different corrosion products formed in this specific area, which are possibly lead chlorite, copper chlorite or copper oxide (to be approved with µXRD analysis).

Figure 45. Coin_4, SEM-EDS backscattered electrons image of lead inclusion

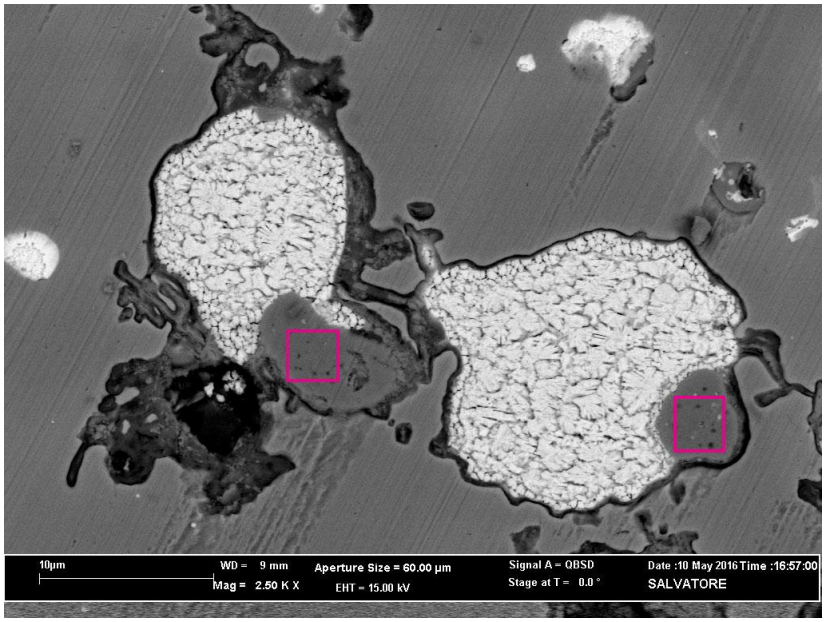

The image of Figure 45 represents a specific area of interest with occurrence of another phase probably formed during the process of coin casting. It appears as a solid phase composed of copper and lead. Two areas of this Cu-Pb formation are highlighted on the same image. The following EDS spectrum reveals the elemental composition of one of the spots, consisted of copper and lead elements.

Figure 46. Coin_4. EDS spectrum of Cu-Pb phase

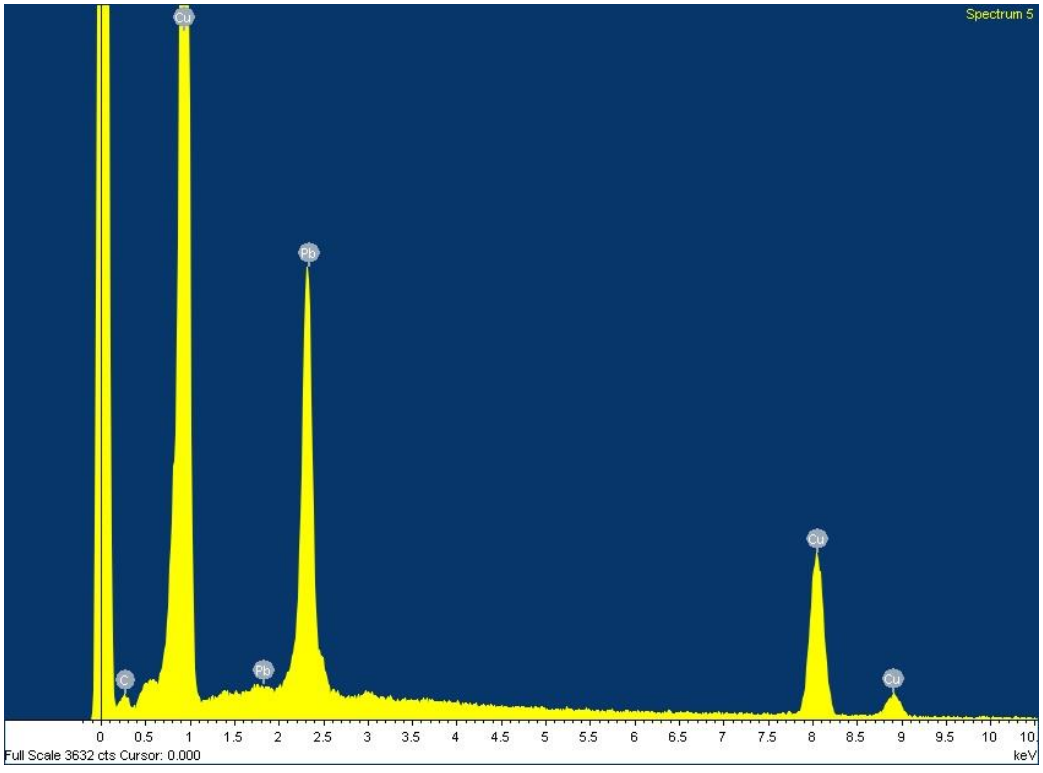

The occurrence of the same specific phase formation is identified in an analysis of Coin_1 sample during the mapping performed with Merlin Scanning Electron Microscope and described above.

XRF analysis results of Coin_4 bulk bronze alloy showed that the elemental composition consists of the same elements and their relation as the Coin_3, with the copper as the major element and the high lead content (around 40 %), presented in a spectrum of Figure 47.

Figure 47. Coin_4 bulk alloy XRF spectrum.

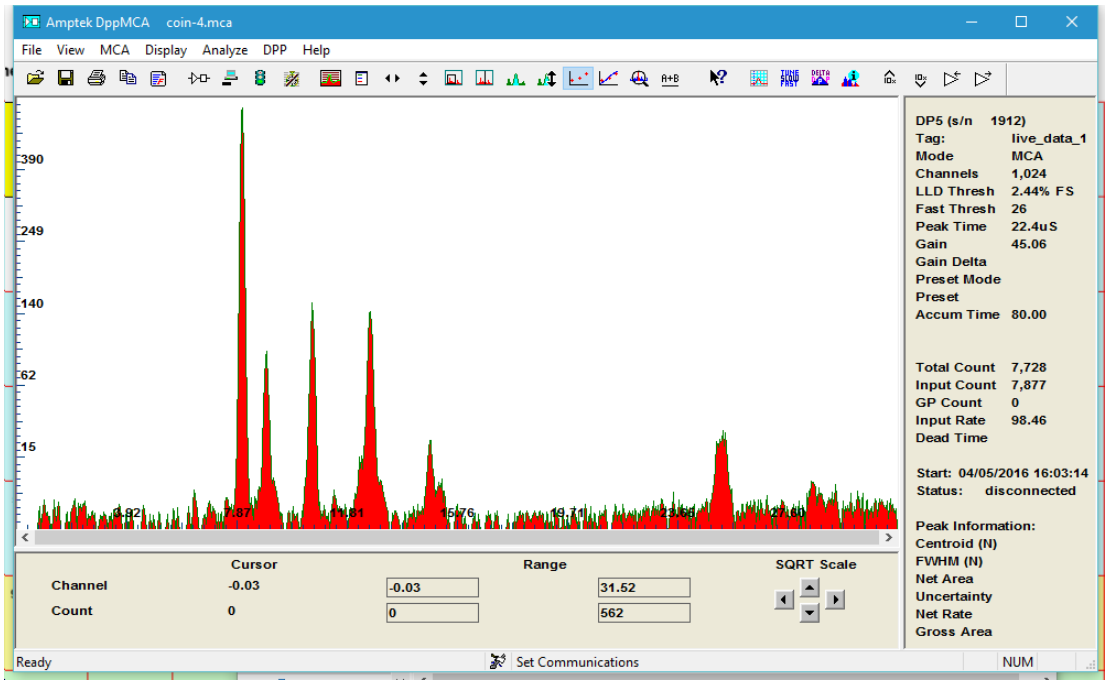

Corrosion analysis

Coin_1

Figure 48. SEM-EDS secondary electrons image of Coin_1 patina

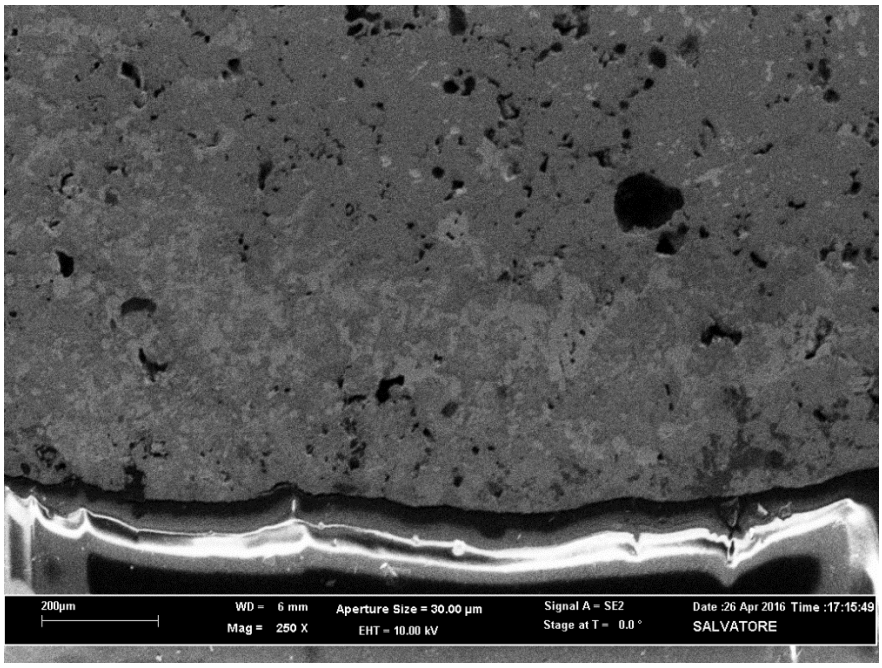

Figure 48 represents the FESEM-EDS image of the Coin_1 patina layer from the cross-section cut edge of the sample, taken with secondary electrons detector with magnification of x250. The thickness of patina is relative small, which is around 2µm. The white layer from the edge is related to the resin.

Figure 49. SEM-EDS image of Coin_1 patina layer from the edge with a crack

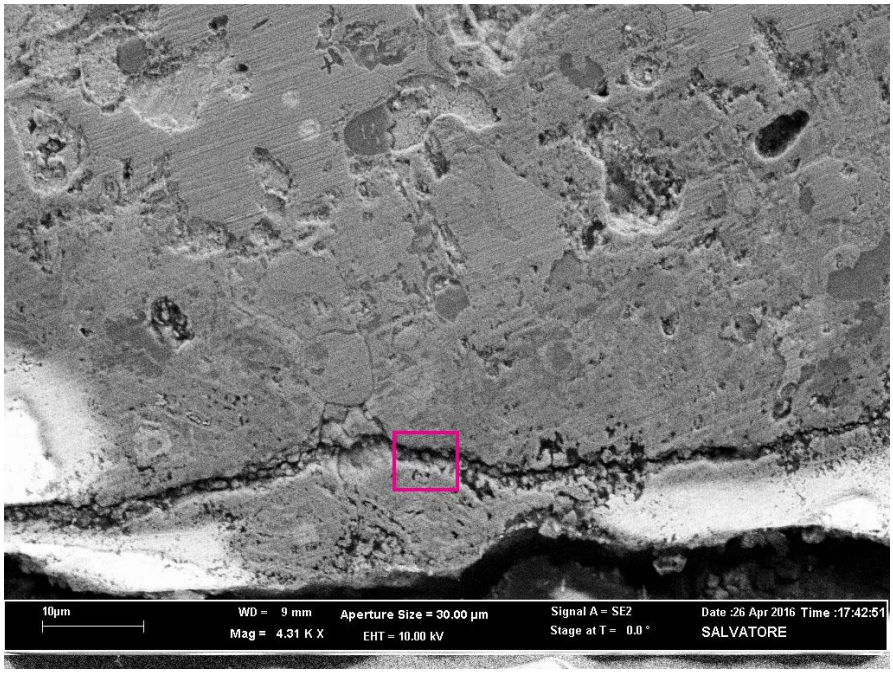

Figure 50. EDS spectrum from the patina spot (Image 2).

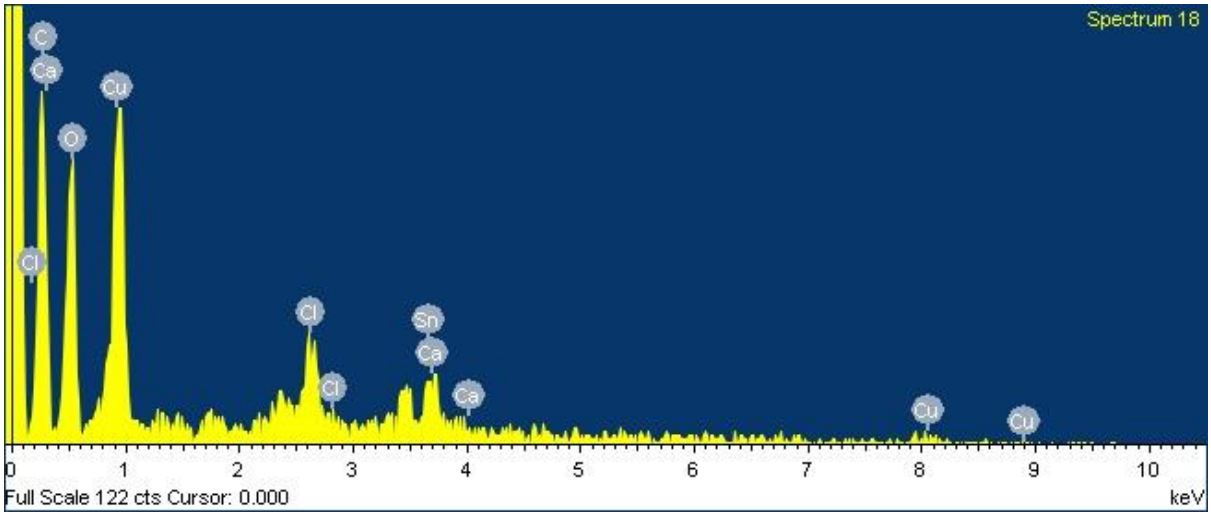

The spot for EDS elemental spectrum (Figure 50) was taken as it is shown on the backscattered image of Figure 49, from the area of crack inside of patina layer on the cut edge of the cross-section of the Coin_1 sample. The image was made with magnification of x4000.

Copper and tin elements are related to a bronze phase of the alloy. Presence of calcium is most probably related to environmental influence from the soil.

XRF analysis of the Coin_1 surface (Figure 51) revealed the peaks of such element like calcium (Kα 3.69, Kβ 4.01). The presence of gold (Lα – 9,71 kV, Lβ – 11,44 kV), which intensity is higher than tin, is related to the golden anode of the X ray tube (spectrum on Figure 54). While the presence of argon is related to the air. These two last elements are present in every spectra and therefore they will not be reported.

Figure 51. Coin_1 surface XRF spectrum.

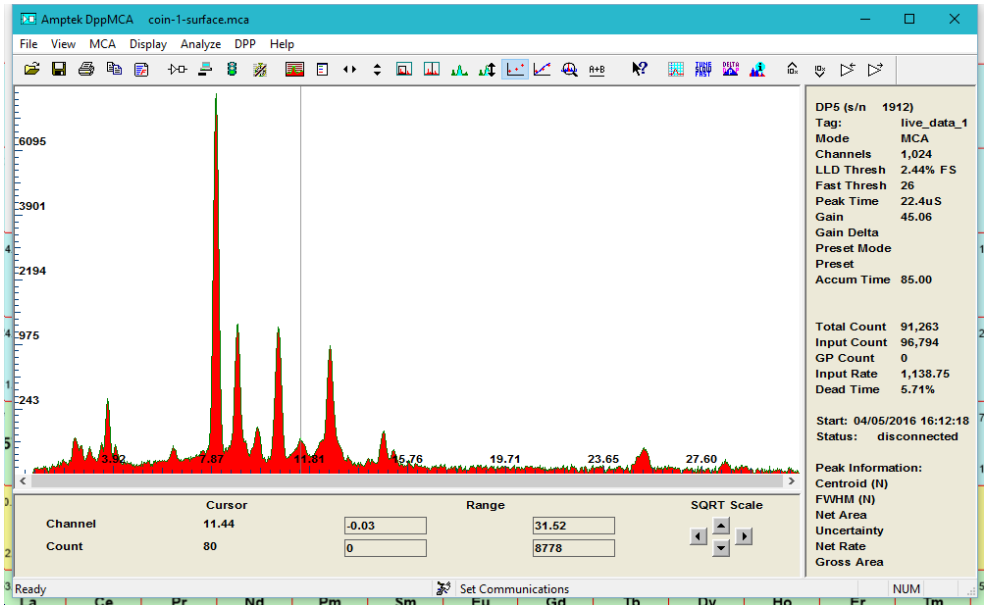

Chlorine is related to patina products as chloride minerals, that is approved by XRD and µXRD analysis of corrosion products, that are discussed further in the chapter.

Figure 52. XRD spectrum of Coin_1 patina. M: malachite, At: atacamite, Co: cotunnite, Cup: cuprite, Cu: copper.

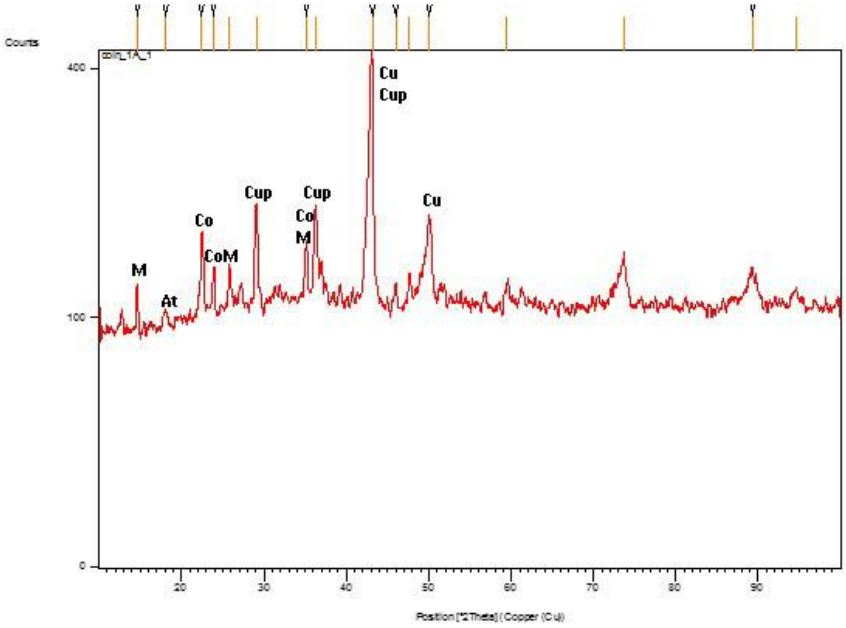

X-ray diffraction spectrum of the Coin_1 patina on the Figure 52 shows the range possibly presented mineral compounds that are defined manually by using database mineral patterns of the most common and expected compounds of bronze corrosion products, and comparing the 2Theta peaks position and intensity of those database compounds with 2Theta peaks of the samples' spectrums.

The XRD examination of patina revealed corrosion products that are known to be normal for archaeological objects made of copper alloys containing lead. Besides of copper alloy itself, XRD spectrum has shown the presence of cuprite Cu_2O, atacamite $Cu_2Cl(OH)_3$, malachite $Cu_2(OH)_3CO_3$ and also cotunnite $PbCl_2$.

Figure 53. µXRD spectrum of Coin_1 patina. P: paratacamite, Te: tenorite, M: malachite, At: atacamite, Co: cotunnite, Cup: cuprite, Cu: copper.

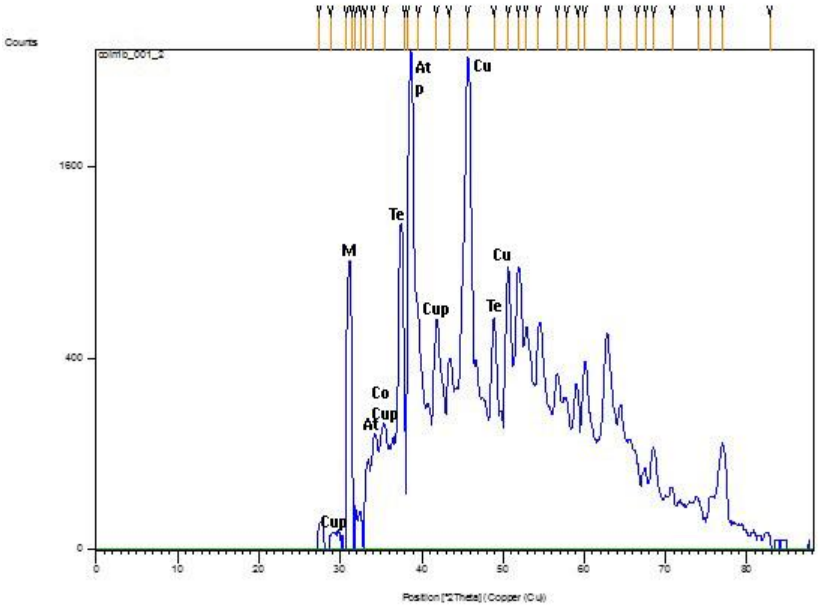

µXRD analysis of small spots (0.3 mm) of corrosion (spectrum of Figure 53) revealed also such minerals as tenorite CuO and paratacamite $Cu_2(OH)_3Cl$.

Figure 54. OM image of the Coin_1 corrosion edge.

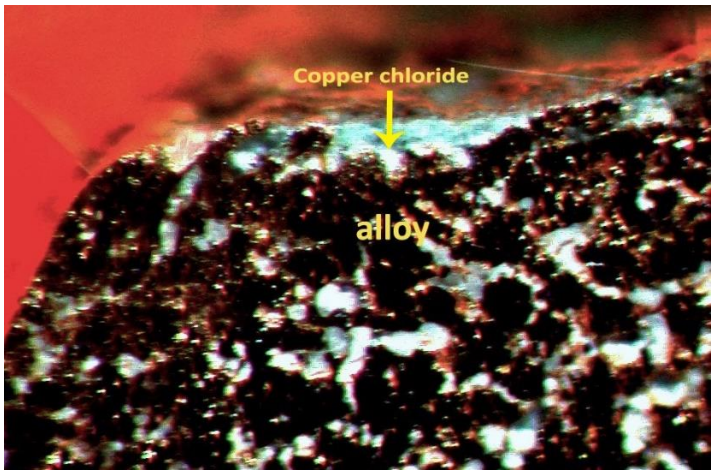

A stereo optical microscopy imaging was performed for a Coin_1 cross-section sample in order to observe the corrosion formation in details. The image of Figure 54 was taken with magnification of x50. Since the Coin_1 was in a quite good preservation state, the corrosion surface layer is thin, around 2µm, as it was discovered by SEM and noticed above. This thin green layer of copper chloride is visible on the OM image above (Figure 54).

Coin_4

Figure 55. SEM-EDS secondary electrons image of patina layer on the cut edge of the cross-section

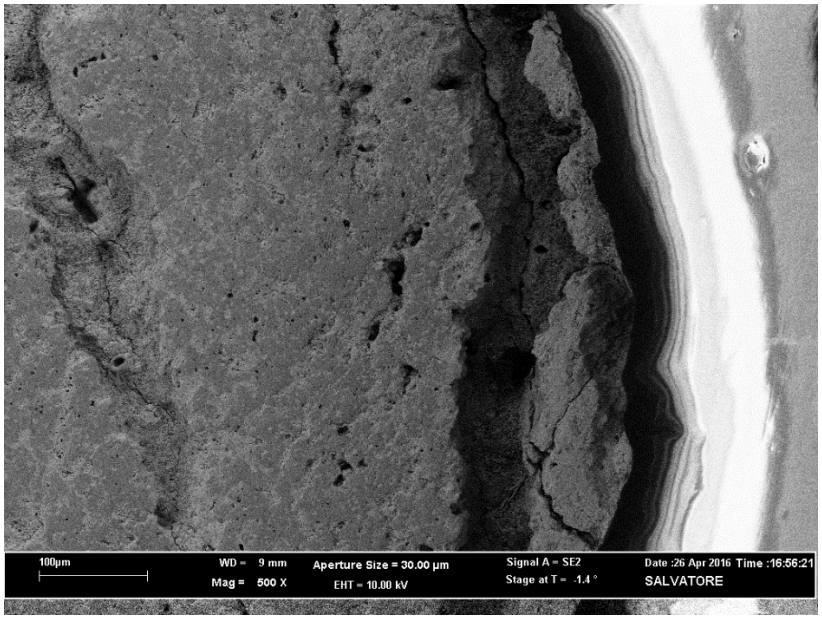

Figure 56. SEM-EDS image of spot analysis from area of corrosion

On the Figure 55 is the SEM-EDS image of corrosion layer on the cut edge of the cross-section of Coin_4 sample, made with magnification of x500 using secondary electrons detector. Since the Coin_4 was in a highly corroded condition, the thickness of patina layer is quite large, comparing with the Coin_1, which was in a relatively good preservation state.

Figure 56 SEM-EDS image represents the crack in an area of corrosion that is visible on a previous image of Figure 55. The spot of EDS analysis for elemental composition is highlighted by a pink frame (Figure 56). The elemental spectrum of this spot is shown by Figure 57.

Figure 57. Coin_4 SEM-EDS spectrum of a spot analysis from a Figure 53.

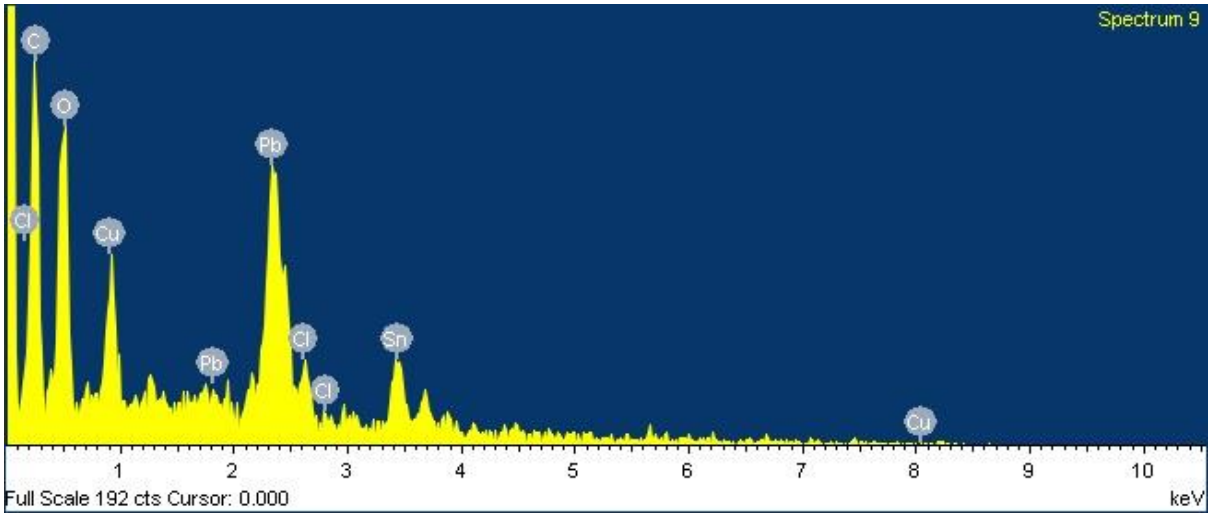

The spectrum reports that the spot of analysis captured an area consisted of two phases of an alloy (Cu-Sn phase and Pb phase), that is evident by presence of high amount of copper, tin and lead. The corrosion products were also presented at the same area, since chlorine is detected, that is probably related to patina 'bronze disease' compounds, which is approved by XRD and μXRD analysis of Coin_4 corrosion products in a discussion following below.

Figure 58. XRD spectrum of Coin_4 patina. M: malachite, At: atacamite, Co: cotunnite, Cup: cuprite, Ce: cerussite, Cli: clinoatacamite

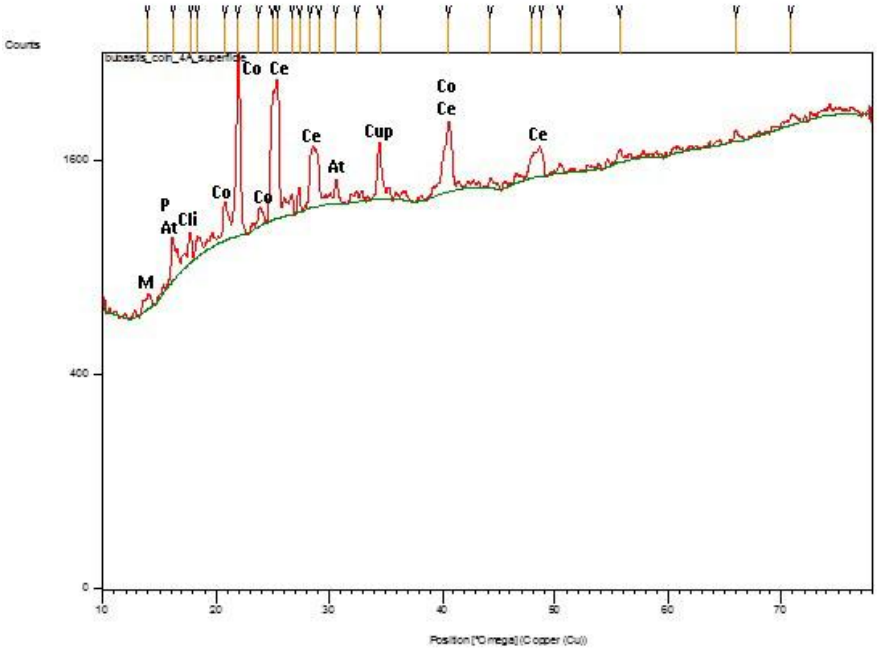

Figure 59. µXRD spectrum of coin_4 patina. At: atacamite, Co: cotunnite, Cup: cuprite, Ce: cerussite, Cli: clinoatacamite, N: nantokite, cchh: copper chloride hydroxide hydrate.

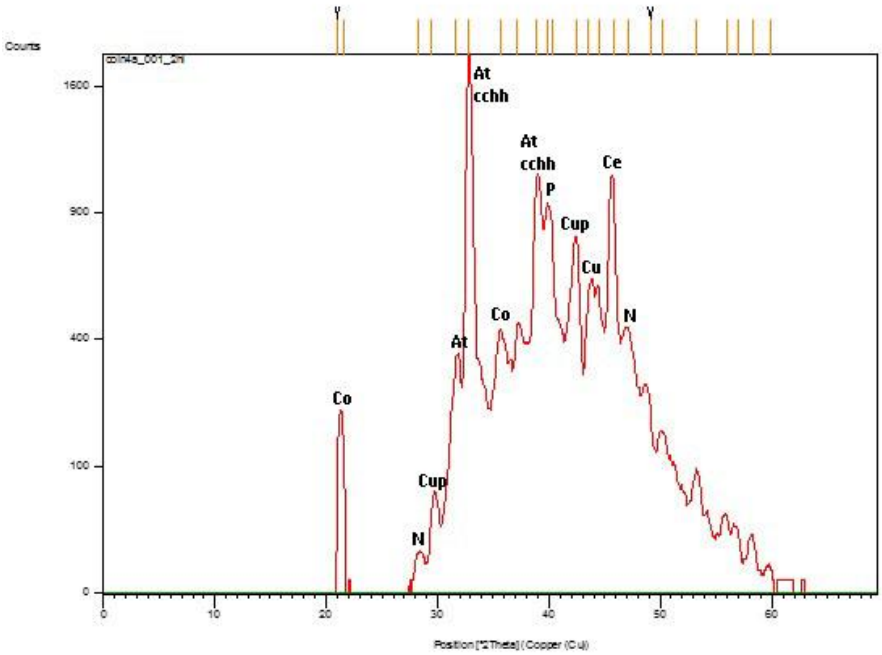

Coin_4 was in an extremely corroded condition when the corrosion products penetrated the metal alloy, which has become almost completely mineralised.

The patina compounds detected by XRD and µXRD (spectrums of Figures 58, 59) are similar to those of the Coin_1 and consist of cuprite, tenorite, atacamite and paratacamite, and also clinoatacamite, and also cotunnite $PbCl_2$ and cerussite $PbCO_3$. Also according to a spectrum results, there is a possible presence of such mineral as nantokite CuCl and a compound of copper chloride hydroxide hydrate $Cu_7Cl_4(OH)_{10}(H_2O)$ in corrosion products.

Figure 60. OM image of coin_4 cross-section, x50.

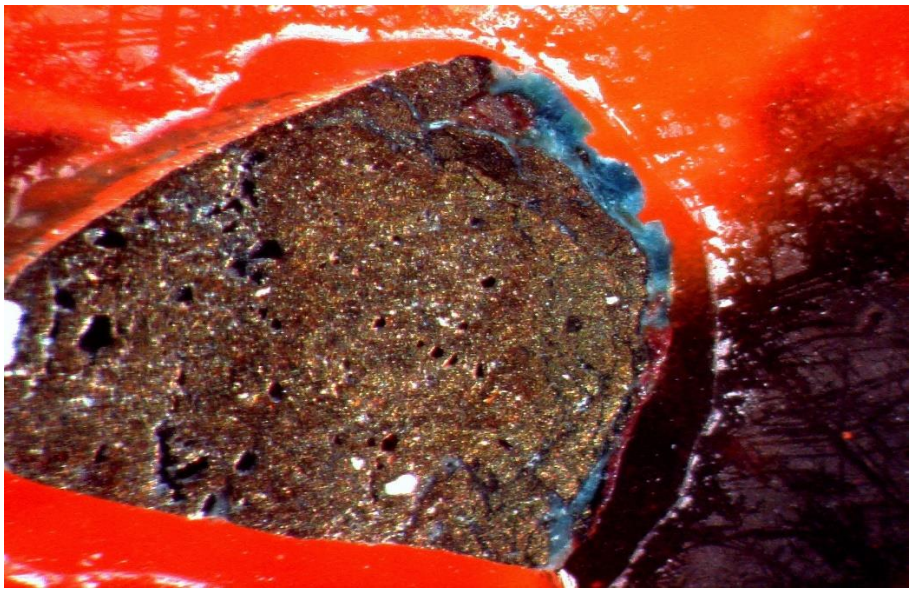

Figure 61. OM image of a corrosion layers of Coin_4, x200.

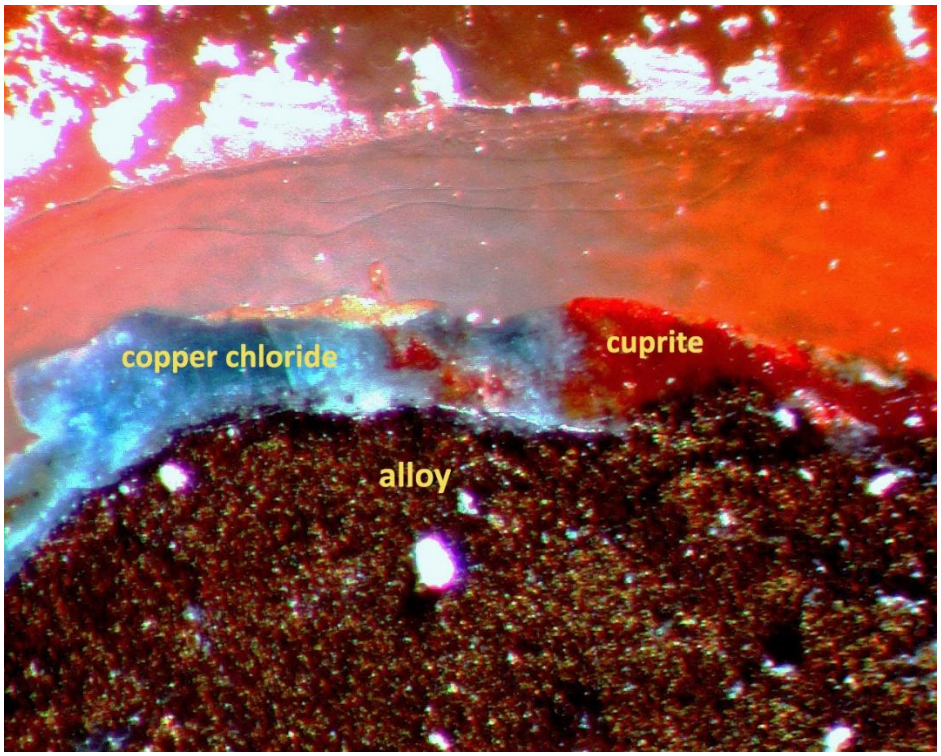

Optical microscopy imaging allows to observe the patina of a coin in a 'real' colours in order to understand more clear the phenomenon of the corrosion formation. Figure 60 represents the general view of the Coin_4

cross-section under the low magnification of x50, and it is possible to see the state of metal preservation, the texture full of cracks and porosity, and the thick layer of surface corrosion.

Figure 61 shows how the corrosion is formed on the surface of bronze alloy, where the greenish layer of copper chloride is banded with a layer of a red copper oxide compound.

Coin_3

The XRF analysis of Coin_3 surface detected range of other elements that are not related to an alloy composition, but to corrosion products, such as iron, cobalt, calcium, sulphur (showed in a spectrum on Figure 62).The presence of cobalt seems to refer to an aesthetic weathering technique.

Figure 62. Coin_3 XRF surface spectrum

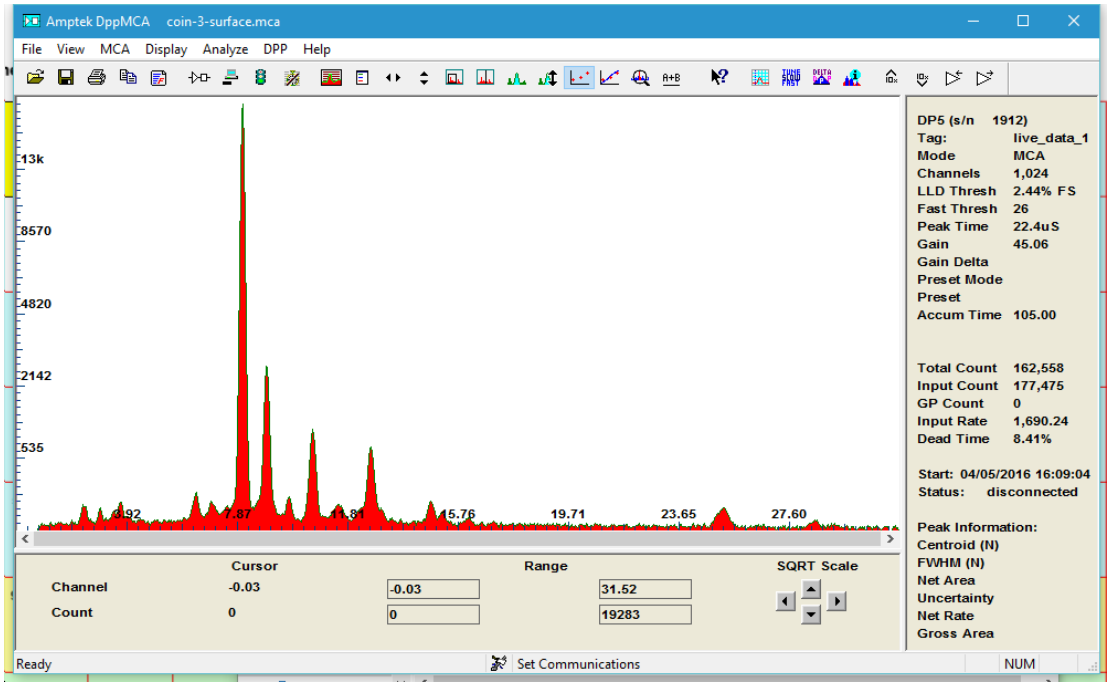

Figure 63. Coin_3. SEM-EDS image of the corrosion spots.

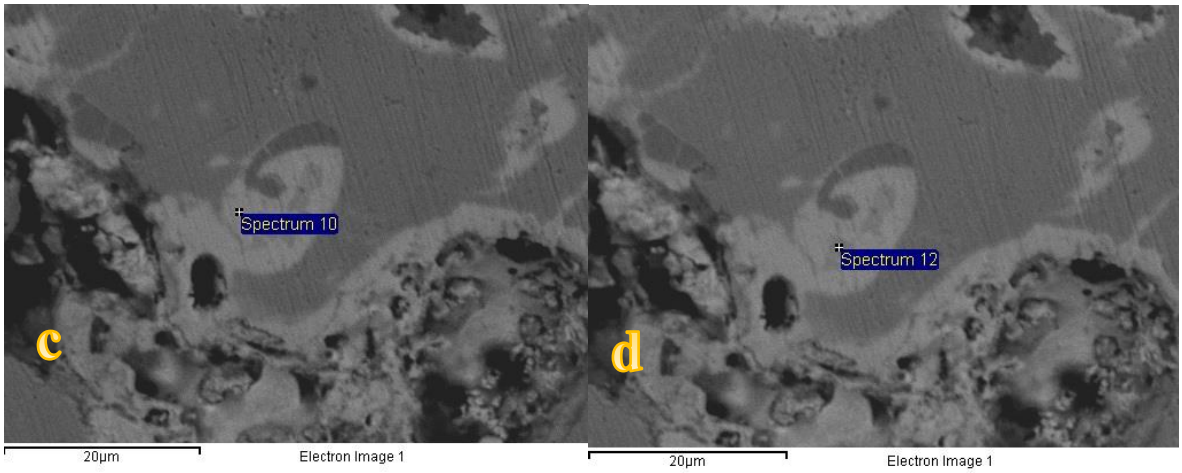

Figure 64. Coin_3, EDS spectrum of a spot of image c (Figure 63)

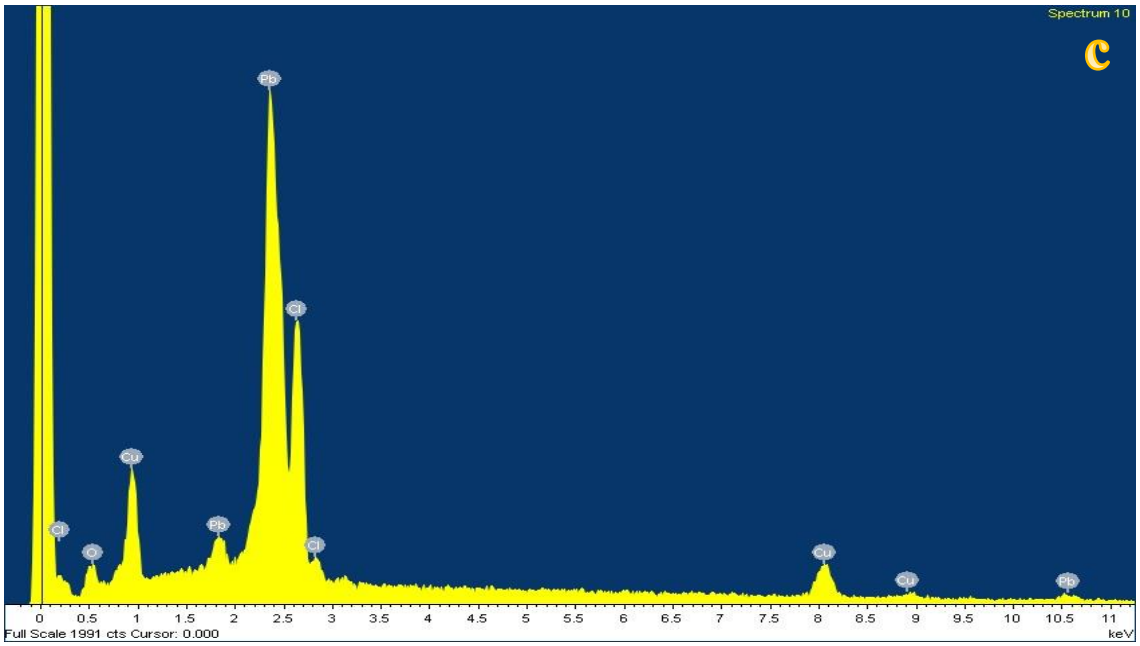

Figure 65. Coin_3, EDS spectrum of a spot of image d (Figure 63).

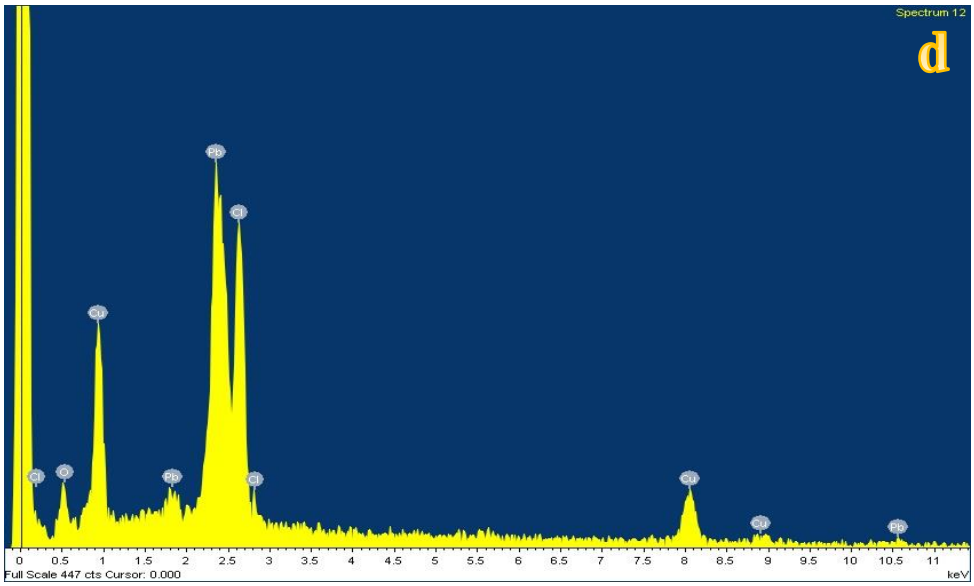

FESEM-EDS corrosion analysis is explained in spectrums of Figure 64 and Figure 65 relevant to analysis of spots **c** and **d** (Figure 63) show the same elemental content, but with difference in peaks intensity which related to a quantitative distribution of elements. The amount of lead is higher in the spot **c**, and lower in the spot **d**, while copper and chlorine are relatively lower in the spot **c** and decrease in the spot **d** spectrum. Chlorine and oxygen are presented possibly due to corrosion formation that usually forms nearby lead inclusions in an alloy. Both spots **c** and **d** probably belong to a particular phase of copper and lead, and the occurrence of this phase is also identified in other coins' samples (Coin_1 and Coin_4).

Figure 66. XRD spectrum of Coin_3 analysis

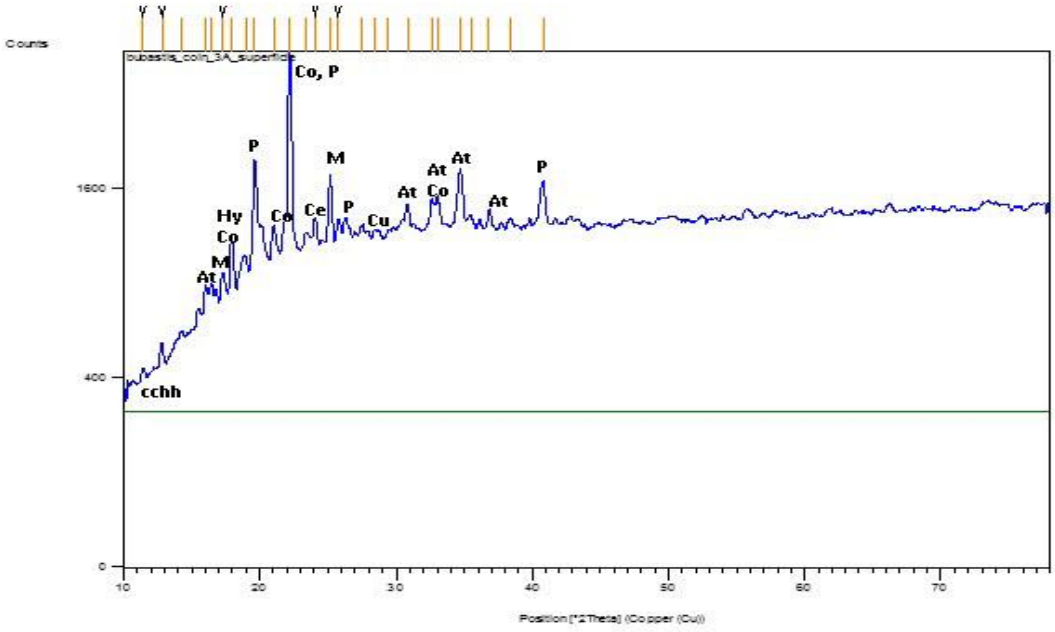

The corrosion products of the Coin_3 were examined with XRD analysis, results of which is comparative with the SEM-EDS compositional data (spectrum of Figure 66).

The Coin_3 was completely mineralised, and XRD analysis showed the presence of range of minerals that are presented in patina of the Coin_4 sample that are malachite, atacamite, paratacamite, cotunnite, cerussite and hydrocerussite $Pb_3(CO_3)_2(OH)_2$, and also copper chloride hydroxide hydrate.

Figure 67. Optical microscopy of Coin_3 corrosion formation, x50.

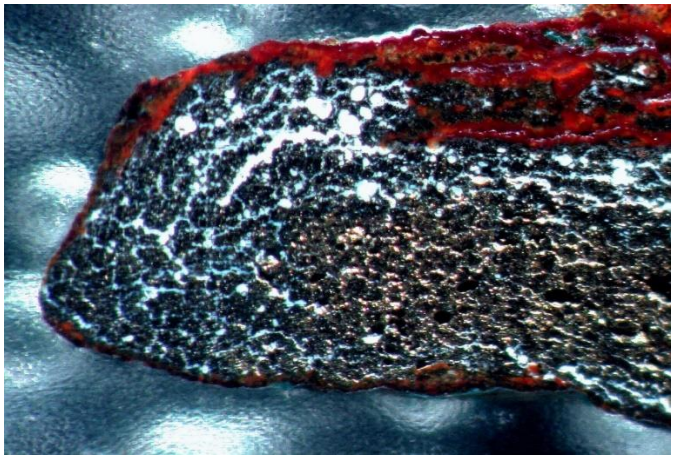

Figure 68. Optical microscopy of the Coin_3 corrosion layers, x200.

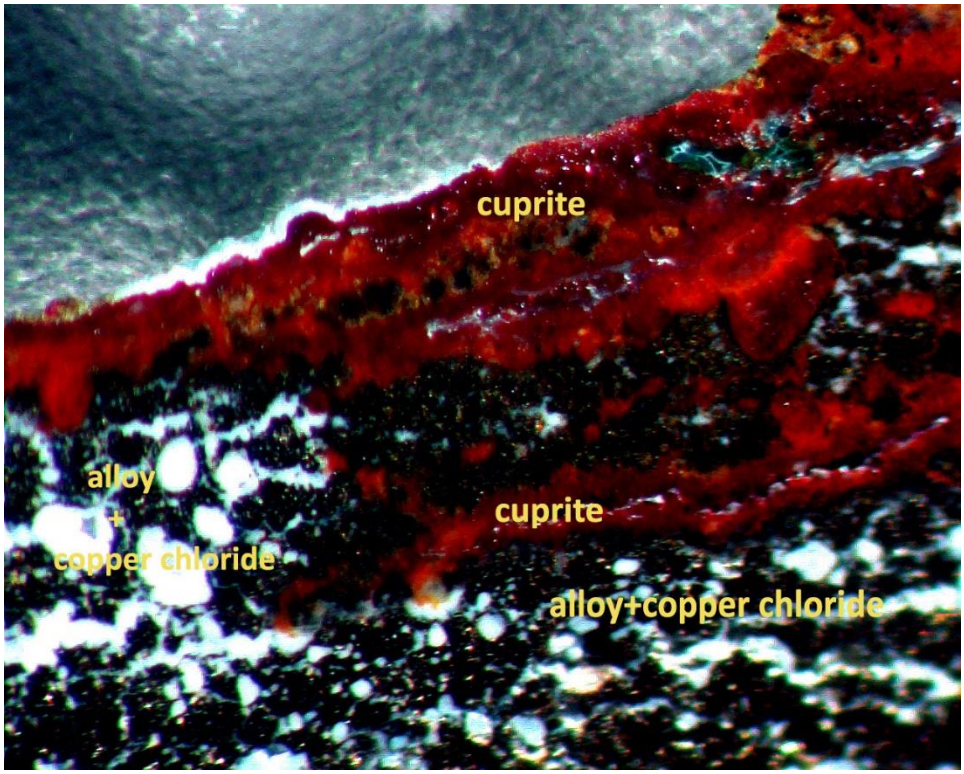

The corrosion of Coin_3 represented in several layers structure can be observed on a stereo optical microscopy images of Figures 67 and 68. The general picture of corrosion formation can be seen with low magnification of x 50 (Figure 67). The red layer of cuprite surrounds the sample surface. Internal corrosion is represented in a formation of green and black layer of copper chloride penetration, so that the coin was almost completely mineralized, but the bulk alloy is partially preserved from inside part of the coin in a goldish layer, which can be observed on a Figure 62.

Higher magnification (Figure 68) shows more clearly the multi-layered distribution of corrosion products, when copper chlorides can be seen formed between the layers of red copper oxides (cuprite).

The presence of chloride compounds (nantokite, atacamite, cerussite, etc.) indicates to occurrence of a 'bronze disease' phenomenon which appears in result of after-burial contact of bronze or other copper alloys with chlorides deposited in a soil or salt water, that contaminate the cupreous objects. Nantokite is also considered to be 'the key mineral product and indicates that salt in soil water was perhaps the main corroding factor. It is not at all unusual to find cuprous chloride in ancient corroded bronzes from desert areas or other places where salt is present' [20]. Nantokite can occurred in different areas of the metal object, beginning from its surface to the interior parts of an object [4]. Bronze disease is visible in a range of green colours from light to vivid green, as it is presented on

[20] L. He, J. Liang, X. Zhao, and B. Jiang, "Corrosion behavior and morphological features of archeological bronze coins from ancient China," *Microchem. J.*, vol. 99, no. 2, pp. 203–212, 2011.

coins 1, 3 and 4. The development of bronze disease can be also caused by explosion of bronze objects to conditions of limited oxygen supply and extreme RH [5][21]

The hydroxides and hydrated Cu compounds (malachite, atacamite) that are also related to green coloured patina, were most probably occurred during the long time interaction of soil environment with the bronze objects [6][22].

As it was mentioned in introduction chapter, the previous study of silver coins excavated at the same archaeological site of Bubastis ancient city (performed by M. Ghonein and M. Megahed[23]. It was interesting to compare the analysis of corrosion products could be of similar nature since the environment conditions during the burial were possibly the same. However, the main identified patina compounds of those silver coins silver chloride and copper chloride compounds ($Cu_2(OH)_3Cl$ and AgCl). Also the presence of $CaCO_3$ was detected on the objects' surface.

[21] E. Angelini, S. Grassini, D. Fulginiti, and M. Parvis, "Corrosion phenomena on ancient Hellenistic coins from Egypt."

[22] L. He, J. Liang, X. Zhao, and B. Jiang, "Corrosion behavior and morphological features of archeological bronze coins from ancient China," *Microchem. J.*, vol. 99, no. 2, pp. 203–212, 2011.

[23] M. Ghonein and M. M. Megahed, "Treatment and conservation of a group of roman coins discovered in Tell Basta, Egypt," in *4th International Congress on Science and Technology for the Safeguard of Cultural Heritage in the Mediterranean Basin*, 2009.

Metallography results

In order to reveal the microstructure of the bulk alloy of the coin sample, the etching was performed, applying 2 drops of the etching solution (the chemical composition and proportion of compounds was described above) each time for 10 seconds. After every time of metallographic attack the solution was rinsed with a distilled water and dried. Microscopic observation was being done after every 10 seconds round of etching until the first results became visible and it was possible to see the metallic microstructure in details.

Figure 69. Coin_1, x500, dendritic structures, 30 seconds etching

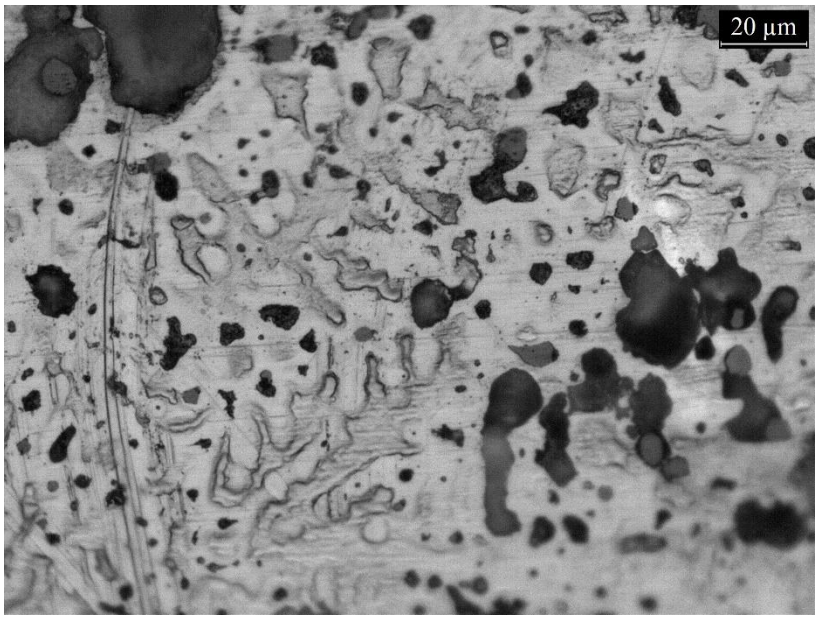

Figure 70. Coin_1, x1000, dendritic structures, 30 seconds etching

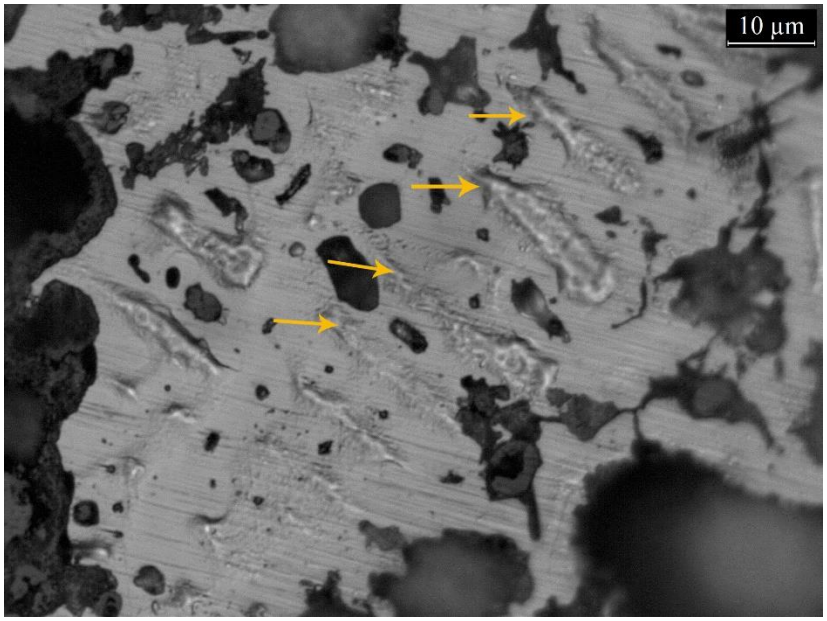

Figure 71. Coin_1, x200, dendritic structures, 50 seconds etching

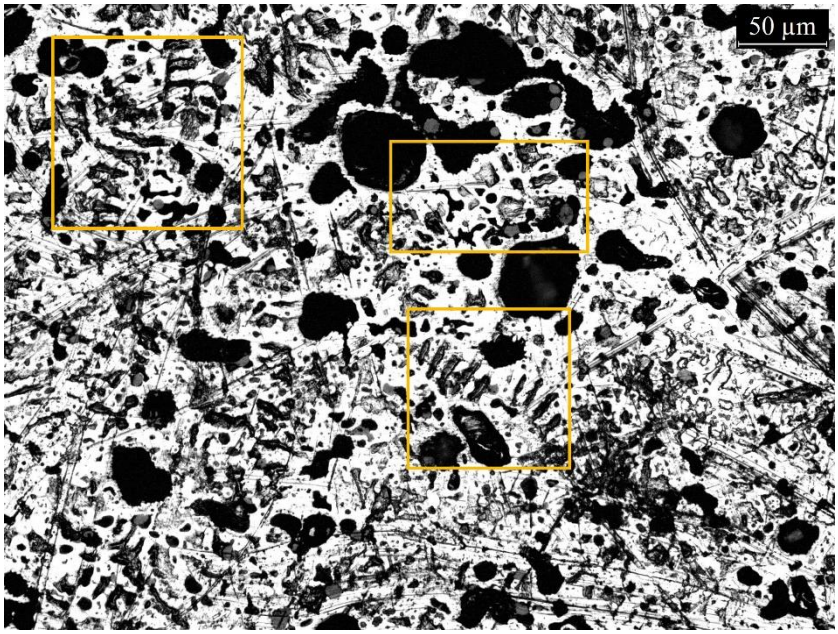

The first etching testing revealed the microstructure of the metal alloy of the *Coin_1,* where it is possible to clearly identify the dendrites captured on the *Figure 69* and *Figure 70,* with a x500 and x100 magnification, after applying the etching solution for 30 seconds in general. The dendrites can be described as coarse, possibly formed on a not very fast cooling rate after casting, and they most possibly belong to a tin-copper solid solution of bronze alloy, where the solvent is copper and the solute is tin. *Figure 71* depicts the microstructure with lower magnification of x200, the dendritic elements are highlighted.

Dendritic structure is one of the common types of microstructure that appear as a result of casting and cooling processes, and dendrites are usually identified in a great majority of ancient metal objects. In most cases dendrites are formed in impure metals due to the fact that one of the components has higher melting point than another one[24] (for example, melting point of copper is 1083° C and tin - 232^0 C). The formation and size of dendrites depend on a rate of cooling, which means that the faster cooling is - the smaller are dendrite elements formed. With a fast cooling rate dendrites can appear in different shapes, having arms – primary, secondary and tertiary. In a case of the Coin_1 dendrites have only primary arms, which probably means that the cooling rate was not extremely fast, but not also not slow, because with a slow cooling dendrites cannot be visible.

The obtained microscopic images are comparable with related examples of artificial alloy metallographic samples (made by researchers of American society of metals [25]): 'high-leaded tin bronze liner (AMS 4825, 74Cu-16Pb-10Sn), gravity cast against inside surface of cylindrical steel shell (bottom). Cored, coarse dendrites of solid

[24] [2] P. T. Craddock, "Metallography and microstructure of ancient and historic metals," *Endeavour*, vol. 16, no. 3, p. 152, 1992.
[25] [1] J. R. Newby, *ASM Handbook volume 9: Metallography and microstructures*. 1985.

solution of tin copper; interdendritic particles of lead (black)'[1]. Reference pictures were acquired with the same etching solution ($NH_4OH + H_2O_2$) and 100X magnification.

Figure 72. Coin_1, x200, lead inclusions, 190 seconds etching

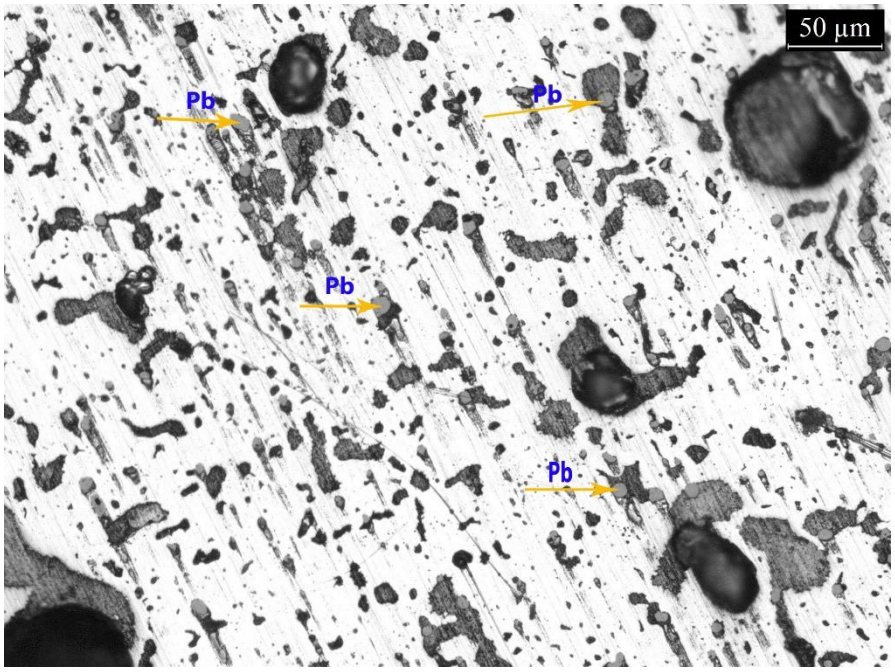

Figure 73. Coin_1, x500, lead inclusions, 190 seconds etching

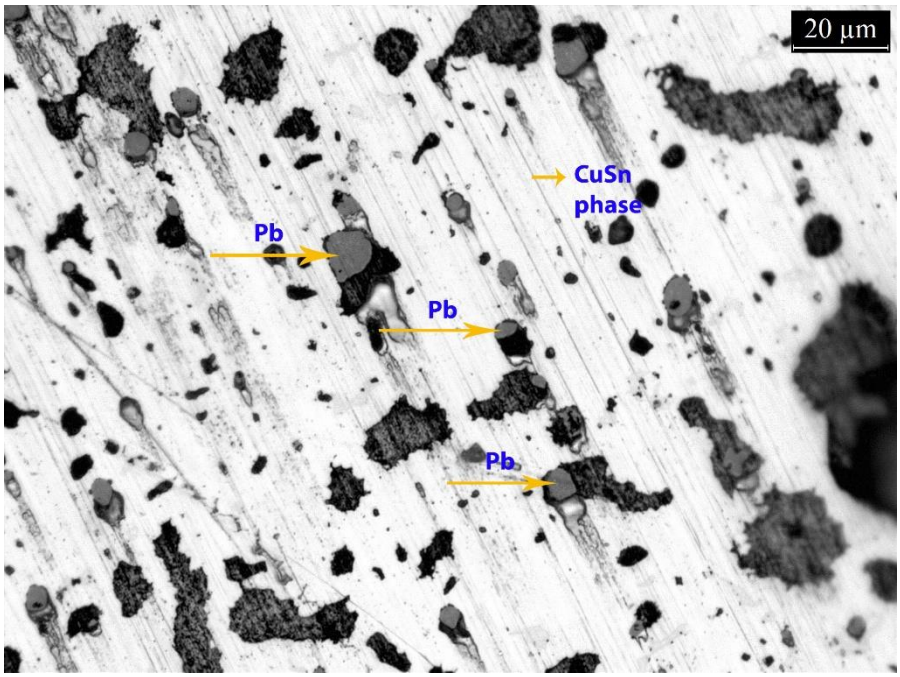

Figure 74. Coin_1, x100, dendrites highlighted on a side of the cross-section, 190 seconds etching

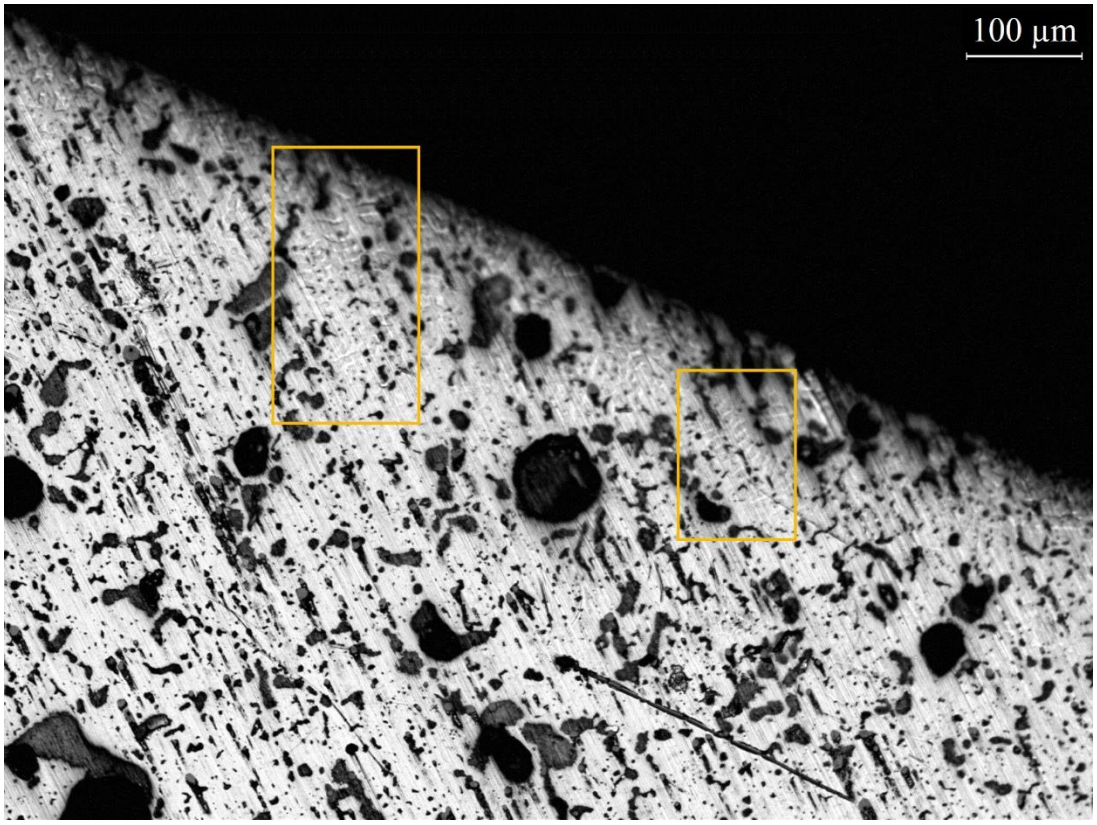

The second session of etching procedure with a sample of *Coin_1* required 190 seconds in total etching time that resulted in revealing of dendritic microstructure, slightly visible on the edge of cross section, the area of which is more sensitive to the chemical impact of etching solution than areas closer to centre. Primary armed dendritic figures are captured on a *Figure 74* with a magnification of x100.

Pictures of *Figure 72* and *Figure 73* were made with x200 and x500 magnification after 190 seconds of total etching time, depict the matrix of metal alloy and microstructure. The Cu-Sn solid phase can be observed in light grey colour (highlighted as *CuSn phase* on a *Figure 73*). The inclusions of lead are clearly visible as dark grey small spots, pointed in *Figure 72* and *Figure 73*. The other dark or black spots represent bores in a structure and most probably refer to corrosion damage affect or mechanical defects of production process of casting.

Conclusion

The present thesis research is focused on archaeometallurgical characterisation of the three bronze coins found in Tell Basta archaeological site, which is ancient Egyptian city Bubastis and located in a Delta region of Nile, not far from modern Zagazig city. After a bibliographic review and a numismatic research, the examined coins were identified as examples of Ptolemaic coinage system of Provincial part of Roman Empire in Alexandria. One of the coins (Coin 1) most possibly belongs to a period of Antoninus Pius emperor (138-161 A.D.), other two (Coin 3 and Coin 4) were probably minted in the 3rd century A.D. under rule of such emperors as Maximinus I (ruled in 235 to 238 AD), Numerian (282-284 AD of reign) or Maximian (286-305 AD of reign). Since the coins were in a critical heavy corroded state, when the legend of a coin and all the obverse and reverse signs were damaged during the burial time, there is no possibility of more precise origin identification.

The objects study was carried out with and multianalytical approach of archaeometry techniques combination, such as X-ray diffraction (XRD), X-ray fluorescence (XRF), optical microscopy (OM), scanning electron microscopy (SEM) and energy dispersive spectrometry (EDS), that were used to identify the elemental composition and microstructure of the bulk metal and to determine the corrosion products.

The results of compositional measurements, performed with a use of XRF and SEM-EDS analysis, showed that the bronze composition of all the three coins consists of copper, tin and lead, with a very high concentration of lead and with a tin as a minor element in an alloy composition.

The study of corrosion products with a use of such techniques as XRF, SEM-EDS, XRD and µXRD, Optical microscopy revealed the presence of oxides, mainly copper oxides, that create the red coloured corrosion crust. The presence of chloride compounds (nantokite, atacamite, cerussite, etc.) indicates to occurrence of a 'bronze disease' phenomenon which appears in result of after-burial contact of bronze or other copper alloys with chlorides deposited in a soil or salt water, that contaminate the cupreous objects.

The research performed has brought new light for the numismatic research, providing data on morphological description and hypothesis of coins identification. The information achieved can be also useful in understanding the economic processes during the times of Roman Empire, which are still not fully discovered. The study of the present conservation state of ancient Roman bronze can lead to recommendations for subsequent methods and ways of conservation treatments of the same or similar cultural heritage objects.

The study of those ancient Roman bronze coins might be continued and completed more due to some thoughts and ideas that would contribute more fully to the scientific fields of numismatic, historical and material studies. More knowledge about the objects is required to identify the exact period of their manufacture and to prove the authenticity of coins themselves. The interpretation of metallographic data acquired during laboratory work of the research is necessary in order to reveal more information on characterisation of the metal alloy microstructure with observation of its features as crystallographic texture and alloy matrix, various inclusions and other properties

of metal alloy. Understanding of metallographic features can help in determining of mechanical and thermal processing of an object, and subsequently the knowledge of manufacturing techniques can contribute to numismatic, historical and economics studies.

Bibliography

Aarts, J. (2005). Coins, money and exchange in the Roman world. A cultural-economic perspective. *Archaeological Dialogues*, *12*, 1. http://doi.org/10.1017/S1380203805211625

Agostino, R., Fracassi, F., Palumbo, F., Angelini, E., Grassini, S., Rosalbino, F., & Inorganiche, M. (2005). Protection of Silver-Based Alloys from Tarnishing by Means of Plasma-Enhanced Chemical Vapor Deposition, 91–96. http://doi.org/10.1002/ppap.200400031

Angelini E., Bianco P., Rosalbino F., Z. F. (1995). A comparative study of methods for the assessment of recovery techniques for aged copper. *Science and Technology for Cultural Heritage*, 1–10.

Angelini, E., Civita, F., Corbellini, S., Fulginiti, D., Giovagnoli, A., Grassini, S., & Parvis, M. (2016). Innovative monitoring campaign of the environmental conditions of the Stibbert museum in Florence. *Applied Physics A*, *122*(2), 123. http://doi.org/10.1007/s00339-016-9635-4

Angelini, E., Grassini, S., Parvis, M., Angelini, E., Grassini, S., & Parvis, M. (2016). Silver artefacts : plasma deposition of SiO x protective layers and tarnishing evolution assessment Silver artefacts : plasma deposition of SiO x protective layers and tarnishing evolution assessment, *2782*(March). http://doi.org/10.1179/147842210X12767807773484

Angelini, E., Ingo, G. M., De Caro, T., & Grassini, S. (2003). Identificazione di Osservabili utilia all'individuazione dei reperti metallici di interesse archeologico, 1–5.

Argyropoulos, V., Angelini, E., & Degrigny, C. (2004). Innovative conservation approaches for monitoring and protecting ancient and historic metals collections from the Mediterranean Basin, (October), 43–52.

Artioli, G. (2010). *Scientific Methods and Cultural Heritage: An Introduction to the Application of Materials Science to Archaeometry and Conservation Science*. *Scientific Methods and Cultural Heritage: An Introduction to the Application of Materials Science to Archaeometry and Conservation Science* (Vol. 9780199548). http://doi.org/10.1093/acprof:oso/9780199548262.001.0001

Beibei, G. U. O. (2014). Tarnish Testing of Copper-Based Alloys Coated with SiO 2 -Like Films Results and discussion, *16*(5), 486–490. http://doi.org/10.1088/1009-0630/16/5/08

Burnett, A., Amandry, M., & Ripollès, P. P. (1992). *Roman Provincial Coinage*. *Roman provincial coinage* (Vol. 1.2).

Butcher, K., & Ponting, M. (2005). KEVIN BUTCHER AND MATTHEW PONTING THE ROMAN DENARIUS UNDER THE JULIO-CLAUDIAN EMPERORS : MINTS , METALLURGY AND TECHNOLOGY, *24*(2), 163–197.

Corsi, J., Grazzi, F., Giudice, A. Lo, Re, A., Scherillo, A., Angelici, D., … Barello, F. (2016). Compositional and microstructural characterization of Celtic silver coins from northern Italy using neutron diffraction analysis ☆ *126*, 501–508. http://doi.org/10.1016/j.microc.2016.01.006

Craddock, P. T. (1992). Metallography and microstructure of ancient and historic metals. *Endeavour*, *16*(3), 152. http://doi.org/10.1016/0160-9327(92)90083-2

Dionis Diez. Metallography – an Introduction. How to reveal microstructural features of metals and alloys.

http://www.leica-microsystems.com/science-lab/metallography-an-introduction/

D.L. Vagi. (2002). Coinage and History of the Roman Empire. *The Journal of Roman Studies*, *92*, 216–218. Retrieved from http://www.jstor.org.proxy1-bib.sdu.dk:2048/stable/pdfplus/3184886.pdf

de Oliveira, F. J. R., Lago, D. C. B., Senna, L. F., de Miranda, L. R. M., & D'Elia, E. (2009). Study of patina formation on bronze specimens. *Materials Chemistry and Physics*, *115*(2-3), 761–770. http://doi.org/10.1016/j.matchemphys.2009.02.035

Empire, R., & Empire, R. (2003). A SECOND INVESTIGATION INTO THE CHEMICAL COMPOSITION OF THE ROMAN PROVINCIAL (PROCURATORIAL) COINAGE, *1*(November 1998), 45–60.

Faraldi, F., Angelini, E., Riccucci, C., Mezzi, A., Caschera, D., & Grassini, S. (2014). Innovative diamond-like carbon coatings for the conservation of bronzes †, (August 2013), 764–770. http://doi.org/10.1002/sia.5367

Fessmann, J. (1993). Plasma treatment for cleaning of metal parts, *59*, 290–296.

Fracassi, F., Agostino, R., Palumbo, F., Angelini, E., Grassini, S., & Rosalbino, F. (2003). Application of plasma deposited organosilicon thin films for the corrosion protection of metals, *175*, 107–111. http://doi.org/10.1016/S0257-8972

Gettens, R. J. (n.d.). CHINESE BRONZE, (1).

Gliozzo, E., Arletti, R., Cartechini, L., Imberti, S., Kockelmann, W. A., Memmi, I., … Tykot, R. H. (2010). Non-invasive chemical and phase analysis of Roman bronze artefacts from Thamusida (Morocco). *Applied Radiation and Isotopes : Including Data, Instrumentation and Methods for Use in Agriculture, Industry and Medicine*, *68*(12), 2246–51. http://doi.org/10.1016/j.apradiso.2010.07.004

Gouda, V. K., Youssef, G. I., & Ghany, N. A. A. (n.d.). Investigation of Chemical Composition , Structure and Corrosion of Ancient Egyptian Bronze Statues, 1–20.

Grassini, S., Angelini, E., Mao, Y., Novakovic, J., & Vassiliou, P. (2011). Progress in Organic Coatings Aesthetic coatings for silver based alloys with improved protection efficiency. *Progress in Organic Coatings*, *72*(1-2), 131–137. http://doi.org/10.1016/j.porgcoat.2011.04.003

Grassini, S., Ishtaiwi, M., Parvis, M., & Vallan, A. (2015). Design and Deployment of Low-Cost Plastic Optical Fiber Sensors for Gas Monitoring, 485–498. http://doi.org/10.3390/s150100485

Griesser, M., Kockelmann, W., Hradil, K., & Traum, R. (2015). New insights into the manufacturing technique and corrosion of high leaded antique bronze coins. *Microchemical Journal*, *126*, 181–193. http://doi.org/10.1016/j.microc.2015.12.002

Gupta, R., Srivastava, S., Kumar, G. V. P., & Panthi, S. K. (2014). Investigation of Mechanical Properties, Microstructure and Wear Rate of High Leaded Tin Bronze after Multidirectional Forging. *Procedia Materials Science*, *5*, 1081–1089. http://doi.org/10.1016/j.mspro.2014.07.401

Gupta, R., Srivastava, S., Kumar, N. K., & Panthi, S. K. (2016). High leaded tin bronze processing during multi-directional forging: Effect on microstructure and mechanical properties. *Materials Science and Engineering: A*, *654*, 282–291. http://doi.org/10.1016/j.msea.2015.12.068

He, L., Liang, J., Zhao, X., & Jiang, B. (2011). Corrosion behavior and morphological features of archeological bronze coins from ancient China. *Microchemical Journal*, *99*(2), 203–212. http://doi.org/10.1016/j.microc.2011.05.009

Ingo, G. M., De Caro T., Riccucci C., A. E. (2006). Large Scale investigation of chemical composition, structure and corrosion mechanism. *Applied Physics A*, 513–520.

Ingo, G. M., De Caro, T., Riccucci, C., Angelini, E., Grassini, S., Balbi, S., … Vassiliou, P. (2006). Large scale investigation of chemical composition, structure and corrosion mechanism of bronze archeological artefacts from Mediterranean basin. *Applied Physics A: Materials Science and Processing*, *83*(4), 513–520. http://doi.org/10.1007/s00339-006-3550-z

Ishtaiwi, M., Parvis, M., Grassini, S., & Vallan, A. (2014). Innovative Low-Cost Plastic Optical Fiber Sensors for Gas Monitoring, 1–6.

Klein, S., Lahaye, Y., Brey, G. P., & Von Kaenel, H. M. (2004). The early Roman Imperial aes coinage II: Tracing the copper sources by analysis of lead and copper isotopes-copper coins of Augustus and Tiberius. *Archaeometry*, *46*(3), 469–480. http://doi.org/10.1111/j.1475-4754.2004.00168.x

Kosec, T., ??urkovi??, H. O., & Legat, A. (2010). Investigation of the corrosion protection of chemically and electrochemically formed patinas on recent bronze. *Electrochimica Acta*, *56*(2), 722–731. http://doi.org/10.1016/j.electacta.2010.09.093

Kosec, T., Ropret, P., & Legat, A. (2012). Raman investigation of artificial patinas on recent bronze-part II: Urban rain exposure. *Journal of Raman Spectroscopy*, *43*(11), 1587–1595. http://doi.org/10.1002/jrs.4124

Lockyear, K. (2012). KRIS LOCKYEAR DATING COINS , DATING WITH COINS, *31*(2), 191–211.

Manso, M., Schiavon, N., Queralt, I., Arruda, A. M., Sampaio, J. M., & Brunetti, A. (2015). Alloy characterization of a 7th Century BC archeological bronze vase - Overcoming patina constraints using Monte Carlo simulations. *Spectrochimica Acta - Part B Atomic Spectroscopy*, *107*, 93–96. http://doi.org/10.1016/j.sab.2015.03.001

Mantovani, L., Tribaudino, M., & Facchinetti, G. (2016). A mineralogical approach to the authentication of an archaeological artefact: Real ancient bronze from Roman Age or fake? *Journal of Cultural Heritage*, 2–6. http://doi.org/10.1016/j.culher.2016.04.002

K. Marušić, H. Otmačić-Ćurković, Š. Horvat-Kurbegović Comparative studies of chemical and electrochemical preparation of artificial bronze patinas and their protection by corrosion inhibitor. *Electrochimica Acta*, *54*(27), 7106–7113. http://doi.org/10.1016/j.electacta.2009.07.014

Megahed, M. M. (2014). A SYSTEMATIC APPROACH TO BRONZE CORROSION PRODUCTS AND THE METHODS OF TREATMENT, APPLIED ON THREE BRONZE ANKLETS FROM DHAMAR MUSEUM, YEMEN. *Archaeomatica*.

Moreno-Suárez, A. I., Gómez-Tubío, B., Respaldiza, M. A., Chaves, F., Ortega-Feliu, I., Ontalba-Salamanca, M. A., & Ager, F. J. (2011). Combining non-destructive nuclear techniques to study Roman leaded copper coins from Ilipa (II-I centuries B.C.). *Nuclear Instruments and Methods in Physics Research, Section B: Beam Interactions with Materials and Atoms*, *269*(24), 3098–3101. http://doi.org/10.1016/j.nimb.2011.04.077

Muresan, L., Varvara, S., Stupni??ek-Lisac, E., Otma??i??, H., Maru??i??, K., Horvat-Kurbegovi??, S., … Takenouti, H. (2007). Protection of bronze covered with patina by innoxious organic substances. *Electrochimica Acta*, *52*(27 SPEC. ISS.), 7770–7779. http://doi.org/10.1016/j.electacta.2007.02.024

Neri, A., Parvis, M., Perrone, G., Grassini, S., Angelini, E., & Mombello, D. (2009). Low-cost H 2 S gas sensor

based on plastic optical fiber.

Newby, J. R. (1985). *ASM Handbook volume 9: Metallography and microstructures*. *Ed. by GF Vander Voort, ASM Intenational*.

numismaticmanual00akeruoft.pdf. (n.d.).

Palumbo, F. (n.d.). Cultural heritage protection with low plasma treatments, 26–32.

Papadopoulou, O., Vassiliou, P., Grassini, S., Angelini, E., & Gouda, V. (2015). Soil-induced corrosion of ancient Roman brass - A case study. *Materials and Corrosion*, (Xxx). http://doi.org/10.1002/maco.201408115

Plastep, P. (n.d.). Plasma Treatment for Environment Protection, 1–106.

Quaranta, M., Catelli, E., Prati, S., Sciutto, G., & Mazzeo, R. (2014). Chinese archaeological artefacts: Microstructure and corrosion behaviour of high-leaded bronzes. *Journal of Cultural Heritage*, *15*(3), 283–291. http://doi.org/10.1016/j.culher.2013.07.007

Reale, R., Plattner, S. H., Guida, G., Sammartino, M., & Visco, G. (2012). Ancient coins: cluster analysis applied to find a correlation between corrosion process and burial soil characteristics. *Chemistry Central Journal*, *6*(Suppl 2), S9. http://doi.org/10.1186/1752-153X-6-S2-S9

Reynolds, J. (1978). Hadrian, Antoninus Pius and the Cyrenaican Cities. *JRS*. http://doi.org/10.2307/299630

Robbiola, L., Blengino, J. M., & Fiaud, C. (1998). Morphology and mechanisms of formation of natural patinas on archaeological Cu-Sn alloys. *Corrosion Science*, *40*(12), 2083–2111. http://doi.org/10.1016/S0010-938X(98)00096-1

Robert, M. F., & Tylor, L. (1972). *Metals Handbook. 8th edition. Volume 7. Atlas of Microstructures of Industrial Alloys* (Volume 7). Ohio.

Rogério dos Santos Alves; Alex Soares de Souza, et all. (2014a). *No Title No Title*. *Igarss 2014*. http://doi.org/10.1007/s13398-014-0173-7.2

Rogério dos Santos Alves; Alex Soares de Souza, et all. (2014b). No Title No Title. *Igarss 2014*, *I*(1), 1–5. http://doi.org/10.1007/s13398-014-0173-7.2

Romano, F. P., Garraffo, S., Pappalardo, L., & Rizzo, F. (2012). In situ investigation of the surface silvering of late Roman coins by combined use of high energy broad-beam and low energy micro-beam X-ray fluorescence techniques. *Spectrochimica Acta - Part B Atomic Spectroscopy*, *73*, 13–19. http://doi.org/10.1016/j.sab.2012.05.012

Ropret, P., & Kosec, T. (2012). Raman investigation of artificial patinas on recent bronze - Part I: Climatic chamber exposure. *Journal of Raman Spectroscopy*, *43*(11), 1578–1586. http://doi.org/10.1002/jrs.4068

Rowan, C. (2013). Imaging the Golden Age: the coinage of Antoninus Pius. *Papers of the British School at Rome*, *81*(September 2013), 211–246. http://doi.org/10.1017/S0068246213000093

Sciencetechnology, C. E., & Politecnico, M. P. (2016). Silver artefacts : Plasma deposition of SiOx protective layers and tarnishing evolution assessment, (March). http://doi.org/10.1179/147842210X12767807773484

Scott, D. a. (1990). Bronze Disease: A Review of Some Chemical Problems and the Role of Relative Humidity.

Journal of the American Institute for Conservation, *29*(2), 193–206. http://doi.org/10.2307/3179583

Serghini-Idrissi, M., Bernard, M. C., Harrif, F. Z., Joiret, S., Rahmouni, K., Srhiri, A., … Ziani, M. (2005). Electrochemical and spectroscopic characterizations of patinas formed on an archaeological bronze coin. *Electrochimica Acta*, *50*(24), 4699–4709. http://doi.org/10.1016/j.electacta.2005.01.050

Sutherland, C. H. V. (1984). The Roman Imperial Coinage. London: Sping and Son LTD.

Valério, P., Silva, R. J. C., Soares, A. M. M., Araújo, M. F., Gonçalves, A. P., & Soares, R. M. (2015). Combining X-ray based methods to study the protohistoric bronze technology in Western Iberia. *Nuclear Instruments and Methods in Physics Research Section B: Beam Interactions with Materials and Atoms*, *358*, 117–123. http://doi.org/10.1016/j.nimb.2015.06.011

Wang, J., Xu, C., & Lv, G. (2006). Formation processes of CuCl and regenerated Cu crystals on bronze surfaces in neutral and acidic media. *Applied Surface Science*, *252*(18), 6294–6303. http://doi.org/10.1016/j.apsusc.2005.08.041

Woytek, B. E. (2010). Roman imperatorial and imperial coinage. *Welcome to the Eric P. Newman Graduate Seminar 2010*.

Acknowledgements

I would like to thank my thesis supervisors of the University of Turin Prof. Emma Angelini for accepting my thesis project, and Prof. Sabrina Grassini for her continuous support and valuable advices during my laboratory research.

I would also like to thank my supervisor Prof. Giovanni Gigante of the Sapienza University of Rome for his help and guidance during all the time of my research.

I would also like to thank the experts who were involved into the laboratory part of my research: Prof. Stefano Ridolfi from Sapienza University of Rome and Prof. Marco Parvis from University of Turin.

I thank my colleagues, Ph.D. students of University of Torino Elisabetta di Francia and Ahmed Hemaid Elomda for helping me in laboratory with different techniques and answering my various questions.

And finally, I thank the ARCHMAT consortium for accepting me for this program and for providing me the Erasmus Mundus scholarship under the FPA agreement between EACEA agency of the EU and the University of Evora, which made possible this thesis work.